Journal of Medicinal Chemistry

pubs.acs.org/jmc Article

Discovery of 5-(3-Chlorophenylamino)benzo[*c*][2,6]naphthyridine Derivatives as Highly Selective CK2 Inhibitors with Potent Cancer Cell Stemness Inhibition

Yuanjiang Wang, Zhaodan Lv, Feihong Chen, Xing Wang, and Shaohua Gou*

Cite This: *J. Med. Chem.* 2021, 64, 5082−5098 Read Online

ACCESS | Metrics & More | Article Recommendations | Supporting Information

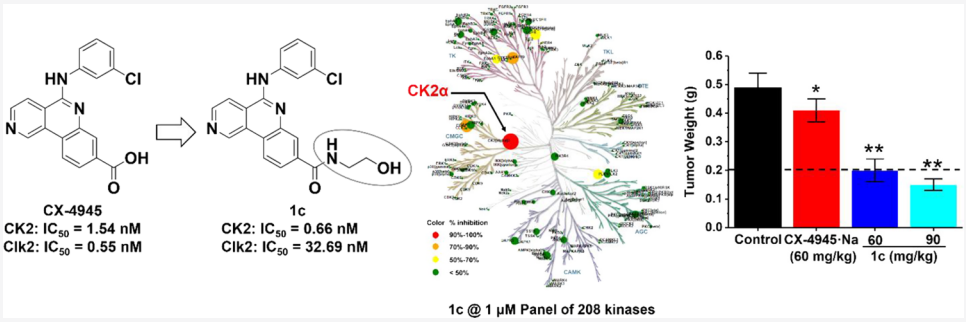

ABSTRACT: Multifunctional entities have recently been attractive for the development of anticancer chemotherapeutic drugs. However, such entities with concurrent CK2 along with cancer stem cell (CSC) inhibitory activities are rare in a single small molecule. Herein, a series of 5-(3-chlorophenylamino)benzo[*c*][2,6]naphthyridine derivatives were synthesized using a known CK2 inhibitor, silmitasertib (**CX-4945**), as the lead compound. Among the resulting compounds, **1c** exhibited stronger CK2 inhibitory activity with higher Clk2/CK2 selectivity than **CX-4945**. Significantly, **1c** could modulate the Akt1(ser129)-GSK-3β(ser9)-Wnt/β-catenin signaling pathway and inhibit the expression of the stemness marker ALDH1A1, CSC surface antigens, and stem genes, showing potent CSC inhibitory activity. Moreover, **1c** also displayed superior pharmacokinetics and antitumor activity compared with **CX-4945** sodium salt, without obvious toxicity. The favorable antiproliferative and antitumor activity of **1c**, its high inhibitory selectivity for CK2, and its potent inhibition of cancer cell stemness make this molecule a candidate for the treatment of cancer.

INTRODUCTION

Casein kinase 2 (CK2), a pleiotropic, acidophilic, and highly conserved serine/threonine protein kinase, plays a crucial role in various essential and pathological biological processes.[1,2] Unlike most other kinases, CK2 is constitutively active and more than 300 substrates are phosphorylated by CK2, making it possibly one of the most pleiotropic proteins in eukaryotic systems.[3,4] It has been confirmed that CK2 is involved in circadian rhythms, gene expression, cell cycle progression, apoptosis, cell growth and differentiation, embryogenesis, and many other cellular processes in a variety of tumors.[5,6] As almost all cancers can be associated with CK2-dependent phosphorylation and tumors rely on CK2 for their survival, cancer cells are more sensitive to CK2 inhibition.[7,8] Significantly, CK2 is constitutively active, but tumor transformation caused by gain-of-function CK2 mutations has not been reported so far. Thus, the widely accepted view is that the increasing levels of CK2 provide a permissive cellular environment that favors malignant transformation through a mechanism referred to as "non-oncogene dependent". Different from classical protein kinase inhibitors, CK2 inhibitors will probably affect multiple targets rather than a single target, leading to an outcome that likely favors cancer treatment.[9]

Consisting of two kinds of subunits, catalytic α/α' along with modulatory β ones, CK2 has large amino acid residues, which make the ATP binding site of CK2 relatively small.[10] Therefore, the ATP competitive inhibitors of CK2 must satisfy two requirements: high specificity and relatively small molecular weight. Researchers have developed a number of CK2 inhibitors including **DRB**, **TBB**, **Emodin**, and **CX-5011** with sub-micromolar Ki values in the past 40 years (Figure 1).[11−14] However, due to the limited selectivity and the weak specificity and potency, apart from the possibly potential long-term toxicity, none of them did fulfill the requirement for successful clinical settings except silmitasertib (**CX-4945**,

Received: January 23, 2021
Published: April 9, 2021

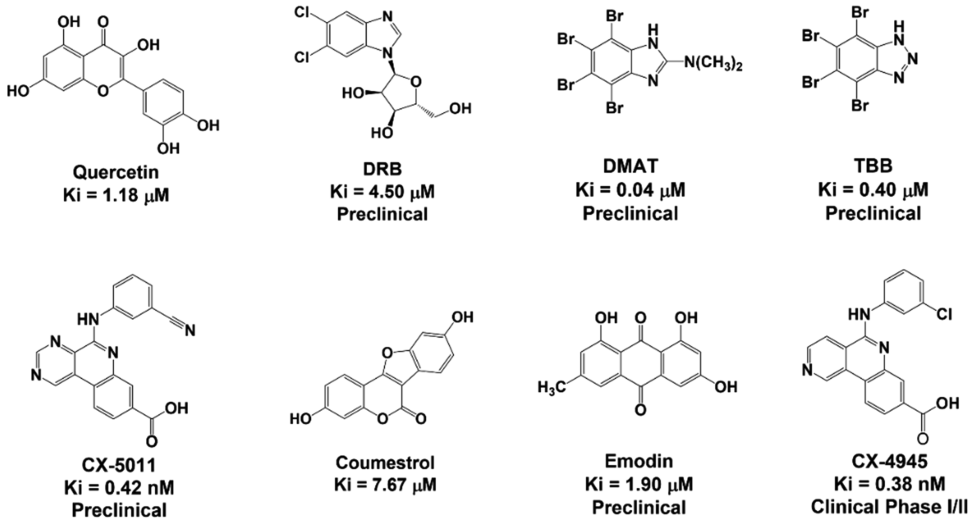

Figure 1. Structures representing known ATP-competitive CK2 inhibitors.

Figure 1). To our knowledge, so far, only **CX-4945** as a small molecule inhibitor of CK2 has entered Phase I/II clinical trials.[6] **CX-4945** has been found to exhibit a strong potency against CK2 with an IC_{50} value of 1 nM; however, unfortunately, it also represses 12 other kinases in nanomolar affinity. Particularly, **CX-4945** has strong inhibition against Clk2, which is even stronger than its inhibition against CK2.[15−17] The potent inhibition of **CX-4945** on Clk2 most likely causes the altered serine/arginine-rich (SR) protein phosphorylation in cells.[18] Although the success of drug development does not always require absolute specificity, cell permeable inhibitors that are highly selective are invaluable tools for studying the role of phosphorylation networks of proteins in the modulation of cellular processes.[19,20]

CK2 has more than 300 phosphorylated substrates that are different signal transduction cascades including Notch, JAK/STAT, PI3K/Akt, Wnt, NF-κB and Hedgehog (Hh).[2] Among them, Wnt/β-catenin, Notch, and Hedgehog/Gli1 are also the main signaling transduction pathways in stem cell biology, providing cancer stem cells (CSCs) with unlimited proliferative capability.[21] CSCs, a small subpopulation of tumor cells, can differentiate into different phenotypes with the ability of continuous self-renewal and differentiation and are a highly tumorigenic subpopulation.[22,23] Unlike most of the tumor cells, CSCs have similar characteristics to stem cells, which are essentially involved in tumorigenesis, tumor recurrence, cancer progression, invasion, metastasis, and therapeutic tolerance.[24,25] Therefore, CSCs provide a new direction for modern cancer research and a critical index for prevention, diagnosis, as well as treatment of cancer.[26] Generally, most of the clinical chemotherapeutic drugs like cisplatin, gemcitabine, and hydroxycamptothecin acting only on common cancer cells have no effect on CSCs, and some even promote the growth of CSCs.[27,28] As a consequence, research and development of targeting drugs to suppress CSCs have been a great challenge and formidable task in cancer research and clinical application.

As stated above, we believe that it is worthwhile to make a reasonable structural modification on the framework of **CX-4945** to obtain novel compounds with increasing anticancer activity and CK2 selectivity and suitable physical and chemical properties as novel CK2 inhibitors. It has been reported that the carboxylic group in **CX-4945** can act as an acceptor or donor to form two essential hydrogen bonds with the amino acid residues near the ATP-binding site in CK2 protein, which accounts for the potent activity of **CX-4945**.[29] Since amide groups can also act as hydrogen bond donors and/or receptors like carboxylic acid, they were selected to modify the skeleton of **CX-4945**. In addition, ester groups were introduced to the framework of **CX-4945** as well. Previous research indicated that CK2 has large amino acid residues that make the ATP binding site of CK2 relatively small.[10] Upon considering the pros and cons of various strategies, some aliphatic amines/alcohols with different side chains were selected to get **CX-4945** derivatives (Figure 2). Herein, we report the synthesis

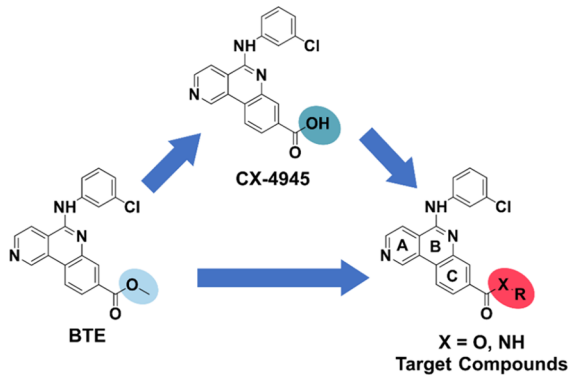

Figure 2. Structure modification strategy for the target compounds.

and biological evaluation of these compounds together with their CK2 inhibition activities and cytotoxicity against a panel of cancer cells. Among the resulting compounds, a potent bifunctional inhibitor (**1c**) was obtained. The inhibition activity of **1c** toward CK2 and CSCs as well as its *in vivo* tumor growth inhibition on an HCT-116 xenograft model was investigated.

RESULTS AND DISCUSSION

Synthesis of Target Compounds. Compounds **BTE** and **CX-4945** were synthesized following the previously documented procedures (Scheme S1).[29] Target compounds were prepared according to the ways shown in Scheme 1. Treatment of **BTE** with hydroxylamine hydrochloride in refluxing

https://doi.org/10.1021/acs.jmedchem.1c00131
J. Med. Chem. 2021, 64, 5082−5098

Scheme 1. Synthesis of Target Compounds

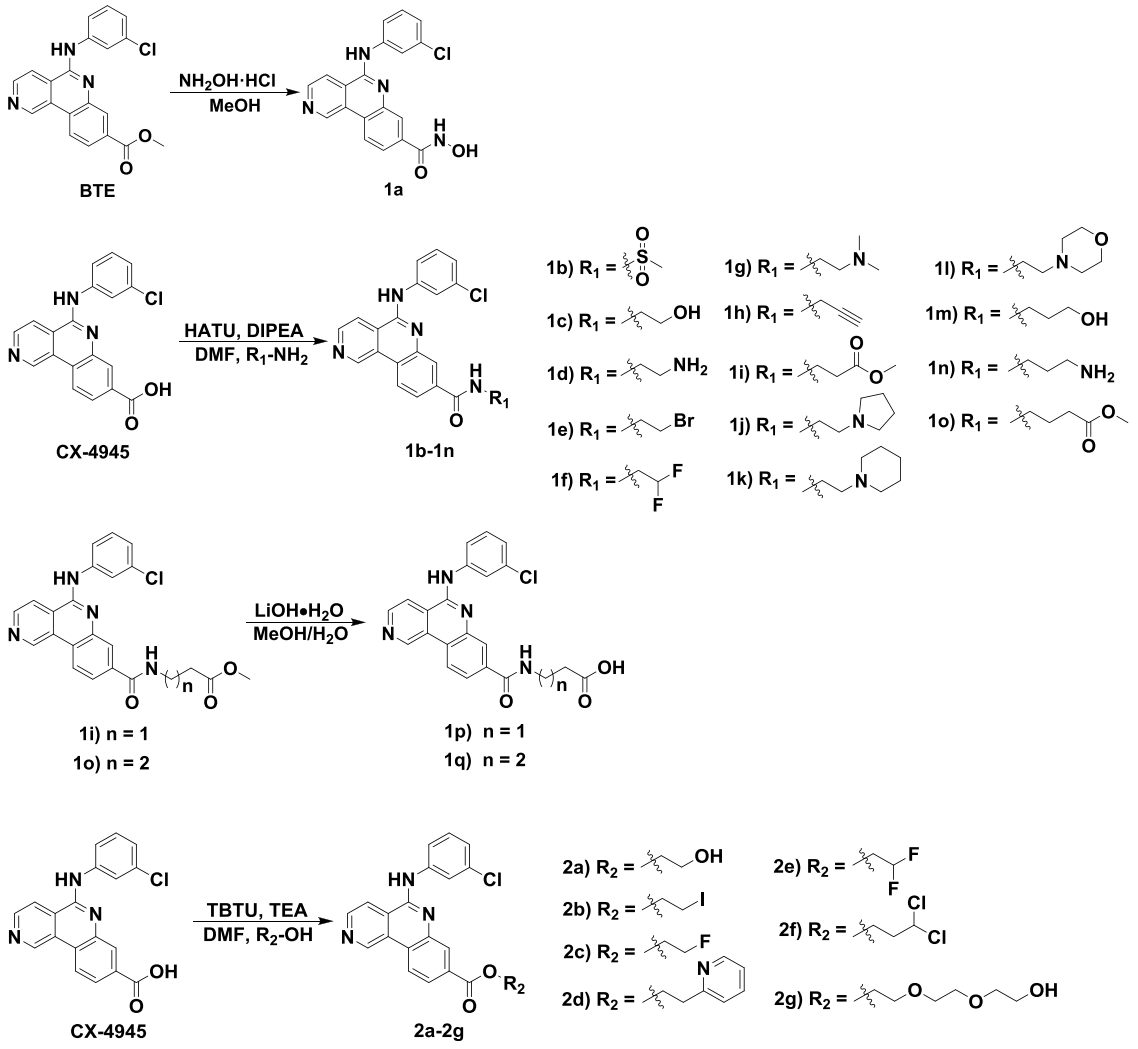

methanol afforded **1a** that precipitated from the reaction mixture upon cooling. Target compounds **1b**−**1o** and **2a**−**2g** were obtained through the condensation reaction of **CX-4945** with different aliphatic amines/alcohols. Compounds **1p** and **1q** were obtained by hydrolysis of **1i** and **1o**, respectively, in the presence of lithium hydroxide.

Physicochemical Properties and Analysis of CK2 and ClK2 Inhibitory Activity. As potential CK2 inhibitors, the inhibitory effects of all the target compounds on CK2 were first detected by a CK2 Kinase (Human) Assay/Inhibitor Screening Assay Kit with **CX-4945** as the positive control. Lipophilic ligand efficiency (LLE) is considered to be an important indicator for predicting absorption, distribution, metabolism, and excretion properties.[30] To find better CK2 inhibitors as potential anticancer agents, we attempted to modulate the LLE values of target compounds while maintaining their CK2 inhibitory effect. Since Clk2 is one of the main off-targets of **CX-4945**, the Clk2 Kinase Assay/Inhibitor Screening Assay Kit was also used to detect those compounds with IC_{50} < 2 nM against CK2. The results are summarized in Table 1. **CX-4945** exhibited a potent inhibitory effect on CK2 but with a small selection factor (SF) for Clk2/CK2. As expected, the introduction of amide with different functional chains could remarkably adjust the CK2 activity of the resulting compounds. Particularly, those containing $-(CH_2)_2-$ chains with potential hydrogen bonding donors and/or acceptors maintained or even enhanced their inhibitory effects on CK2 and decreased their inhibitory activity against ClK2. For instance, compounds **1c**, **1d**, **1i** ,and **1l** have lower IC_{50} values than **CX-4945** against CK2, and the inhibitory effect on Clk2 was also lower than **CX-4945**. **1l** containing a morpholinoethyl group showed the most potent CK2 inhibitory activity (IC_{50} = 0.46 nM). Significantly, its SF value for Clk2/CK2 reached 47.61, which is 136 times over that of **CX-4945**. The inhibitory activity of **1c** containing a 2-hydroxyethyl side chain against CK2 was 0.66 nM with a high selectivity for Clk2/CK2 (142 times higher than that of **CX-4945**). However, compounds **1g**, **1j**, and **1k** displayed weaker CK2 inhibitory effects with IC_{50} values over 10 nM. Although these amide compounds contain a tertiary amine nitrogen atom that can serve as a hydrogen bond receptor, they are less capable of forming hydrogen bonds than those containing an oxygen atom. Introduction of $-(CH_2)_2-$ chains with potential hydrogen bonding donors and/or acceptors like compounds **1m**, **1n**, **1o**, and **1q** seemed not to be beneficial to increase their CK2 inhibitory activity in contrast to **CX-4945**. As for the ester compounds with a $-(CH_2)_2-$ chain containing hydrogen bonding acceptors like **2a**, **2c**, and **2e** and containing a 2-iodoethyl side chain (**2b**), they also exhibited stronger CK2 inhibitory activity than **CX-4945**. Especially, the IC_{50} value of **2c** was 6.67 times less than

https://doi.org/10.1021/acs.jmedchem.1c00131
J. Med. Chem. 2021, 64, 5082−5098

Table 1. Physicochemical Properties and CK2 and ClK2 Inhibitory Activities of the Target Compounds

compound	clogP	LLE[a]	IC_{50} ± SD (nM) CK2	IC_{50} ± SD (nM) ClK2	SF[b]
1a	4.09	4.15	5.66 ± 0.38	NT[c]	
1b	4.32	4.04	9.33 ± 0.23	NT	
1c	4.13	5.05	0.66 ± 0.03	32.69 ± 0.05	49.53
1d	4.21	4.84	0.89 ± 0.07	19.64 ± 0.02	22.07
1e	5.42	3.27	1.78 ± 0.09	24.69 ± 0.07	13.87
1f	5.27	3.10	14.28 ± 0.26	NT	
1g	5.10	3.78	21.30 ± 0.08	NT	
1h	5.11	3.82	18.14 ± 0.05	NT	
1i	5.03	4.07	0.79 ± 0.01	9.7 ± 0.04	12.29
1j	5.74	2.99	16.82 ± 0.02	NT	
1k	5.31	3.59	12.6 ± 0.15	NT	
1l	5.09	4.24	0.46 ± 0.01	21.9 ± 0.08	47.61
1m	4.45	4.55	8.81 ± 0.04	NT	
1n	4.53	4.19	5.32 ± 0.16	NT	
1o	5.36	3.23	4.53 ± 0.15	NT	
1p	4.91	3.83	9.84 ± 0.08	NT	
1q	4.55	4.23	21.65 ± 0.05	NT	
2a	4.53	4.68	0.61 ± 0.02	2.38 ± 0.05	3.90
2b	6.54	2.58	0.76 ± 0.16	1.69 ± 0.08	2.22
2c	5.67	3.97	0.23 ± 0.04	1.06 ± 0.06	4.60
2d	6.02	2.92	7.29 ± 0.11	NT	
2e	5.99	3.23	0.60 ± 0.08	1.54 ± 0.11	2.54
2f	6.50	2.24	3.43 ± 0.56	NT	
2g	4.42	4.45	11.34 ± 0.34	NT	
CX-4945	5.44	3.37	1.54 ± 0.07	0.55 ± 0.02	0.35

[a]LLE was calculated as follows: LLE = pIC_{50} (M) − cLog*P*. [b]SF (selection factor) is defined as IC_{50} (ClK2)/IC_{50} (CK2). [c]NT = not tested.

that of **CX-4945**. However, this kind of compounds did not effectively improve their selectivity for CK2 compared with the corresponding amide compounds. Based on the above structure−activity relationship analysis, we concluded that the amide compounds with a $-(CH_2)_2-$ side chain containing hydrogen bond acceptors and/or donors would be helpful to promote the inhibitory activity and selectivity of the compound against CK2.

Kinase Selectivity Profiling. To demonstrate the inhibitor's kinase selectivity, **1c** was profiled for suppression against a panel of 208 human kinases using the ADP-Glo and HTRF kinase assay. As illustrated in Figure 3 and Table S1, **1c** exhibits the expected high selectivity for CK2α within the human kinome. The activity of CK2α can be completely inhibited by **1c** at 1 μM. It is observed that the inhibition rate of **1c** on Clk2, ZAP70, EGFR(ErbB1), PLK1, and EPHA1 kinases is more than 50% but less than 78%. Among them, the highest inhibition rate of Clk2 is only about 80% (Figure 3c). Overall, compound **1c** exhibits strong and selective inhibition against CK2α.

Investigations on the Antiproliferative Activity *In Vitro*. The antiproliferative influences of all the target compounds against five CK2-overexpressed cancer cell lines (prostate cancer, PC-3; colon cancer, HCT-116 and HT-29; breast cancer, MCF-7; and bladder cancer, T24) together with normal embryonic liver cells (LO2) were assessed by an MTT assay in which **CX-4945** was employed as a positive control. The IC_{50} values derived from the dose−response curves are indicated in Table 2. It was observed that the cell proliferation inhibitory activities of the target compounds were related to their effects on enzyme inhibition. Compounds **1c**, **1d**, **1i**, and **1l** with strong inhibitory potency against CK2 displayed potent antiproliferative influence against the tested cancer cells. For

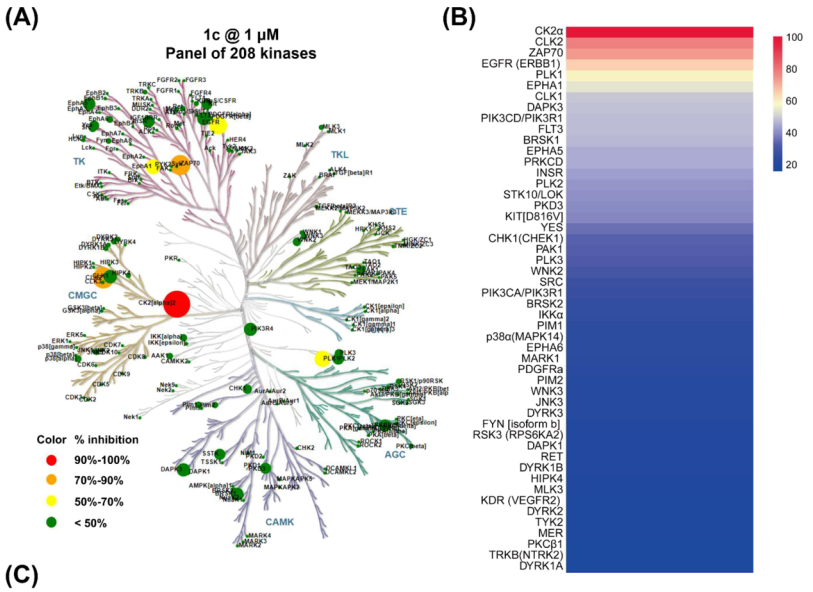

(C)

Targets	CK2α	Clk2	ZAP70	EGFR (ErbB1)	PLK1	EPHA1
1c @ 1μM Activity remaining	0	22.1	26.03	34.12	40.48	45.22

Figure 3. Compound **1c** demonstrates high potency as well as selectivity for CK2α *in vitro*. (a) Graphical illustration of the kinase inhibition profile of **1c** with 208 kinases (a list of the tested kinases is shown in Table S1). The KinMap software tool provided by Cell Signaling Technology, Inc. (https://www.cellsignal.com) was employed to map the TREEspot image. (b) Hierarchical clustering depicting the inhibition ratio of **1c** on the top 50 kinases (the higher the level, the better the inhibitory activity). (c) Kinases' activity less than 50% in the presence of compound **1c** at 1 μM.

https://doi.org/10.1021/acs.jmedchem.1c00131
J. Med. Chem. 2021, 64, 5082−5098

Table 2. *In Vitro* Cytotoxicity Profiles of the Target Compounds against Several Human Cancer Cell Lines[a]

	IC_{50} (μM)					
cpd.	PC-3	HCT-116	MCF-7	HT-29	T24	LO2
1a	15.09 ± 0.15	8.62 ± 0.25	7.66 ± 0.11	9.98 ± 0.19	3.89 ± 0.10	21.42 ± 0.69
1b	4.16 ± 0.09	13.25 ± 0.58	12.16 ± 0.45	17.81 ± 0.70	23.49 ± 0.70	28.43 ± 1.59
1c	4.53 ± 0.43	3.07 ± 0.67	7.50 ± 0.15	5.18 ± 0.12	6.10 ± 0.90	96.68 ± 1.28
1d	5.48 ± 0.31	7.26 ± 0.49	4.88 ± 0.65	11.37 ± 0.38	14.42 ± 0.48	111.13 ± 2.46
1e	8.76 ± 0.11	28.11 ± 1.42	14.86 ± 0.72	8.01 ± 0.12	8.95 ± 0.18	66.73 ± 3.53
1f	6.12 ± 0.56	16.54 ± 0.92	10.43 ± 018	13.95 ± 0.31	18.13 ± 0.35	18.37 ± 0.95
1g	11.08 ± 0.25	12.76 ± 0.78	6.01 ± 0.18	5.08 ± 0.10	5.93 ± 0.10	17.26 ± 0.67
1h	7.60 ± 0.18	21.21 ± 0.96	13.88 ± 0.69	16.43 ± 0.52	18.49 ± 0.26	28.41 ± 2.01
1i	9.94 ± 0.24	8.13 ± 0.92	4.51 ± 0.52	3.52 ± 0.16	10.67 ± 0.29	>200
1j	10.07 ± 0.57	8.79 ± 0.36	8.60 ± 0.10	7.94 ± 0.15	3.23 ± 0.03	16.04 ± 0.93
1k	6.08 ± 0.39	8.60 ± 0.20	3.74 ± 0.06	13.80 ± 0.17	3.24 ± 0.07	14.31 ± 0.70
1l	3.28 ± 0.10	7.98 ± 1.40	11.01 ± 0.15	13.37 ± 0.25	8.73 ± 0.55	37.81 ± 1.74
1m	8.94 ± 0.12	13.68 ± 0.30	7.71 ± 0.13	11.75 ± 0.15	18.80 ± 0.53	74.16 ± 2.40
1n	14.10 ± 0.25	15.92 ± 0.85	19.71 ± 0.54	9.87 ± 0.09	37.28 ± 0.90	84.97 ± 1.23
1o	4.89 ± 0.10	5.91 ± 0.24	19.80 ± 0.70	20.60 ± 0.35	12.93 ± 0.15	89.12 ± 6.26
1p	16.18 ± 0.36	4.60 ± 0.10	24.55 ± 0.96	19.90 ± 0.27	24.42 ± 0.50	72.84 ± 4.53
1q	4.20 ± 0.25	24.77 ± 1.57	19.63 ± 0.98	14.51 ± 0.64	21.14 ± 0.58	32.24 ± 0.82
2a	9.15 ± 0.69	10.91 ± 2.55	15.18 ± 0.28	10.90 ± 0.12	16.61 ± 0.56	45.13 ± 3.20
2b	10.01 ± 0.37	17.73 ± 1.15	10.69 ± 0.39	17.13 ± 0.30	17.48 ± 0.62	43.46 ± 1.60
2c	6.40 ± 0.18	4.28 ± 0.27	5.98 ± 0.22	7.80 ± 0.21	5.91 ± 0.86	57.76 ± 3.16
2d	11.00 ± 0.27	6.91 ± 0.18	10.10 ± 0.30	9.52 ± 0.25	22.53 ± 0.50	24.92 ± 1.26
2e	22.09 ± 1.25	7.52 ± 1.60	9.85 ± 0.80	8.09 ± 0.13	22.73 ± 0.39	83.91 ± 1.18
2f	13.53 ± 0.31	20.83 ± 1.20	14.23 ± 0.85	18.40 ± 0.80	20.62 ± 0.46	21.98 ± 1.05
2g	19.18 ± 0.15	9.71 ± 0.19	13.58 ± 0.20	12.62 ± 0.08	14.08 ± 0.38	30.70 ± 1.39
CX-4945	12.75 ± 0.21	13.21 ± 0.52	15.31 ± 0.45	16.00 ± 0.30	12.92 ± 0.25	22.98 ± 2.52

[a]IC_{50} values were given as the means ± SD of three independent experiments.

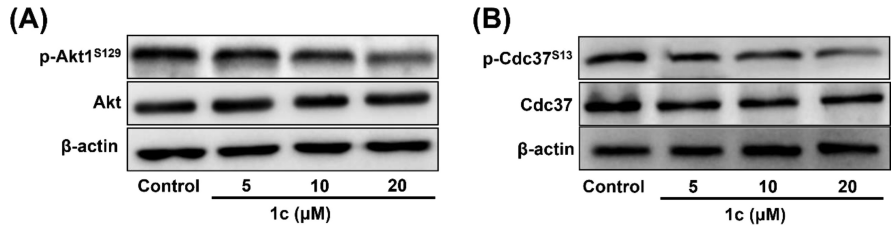

Figure 4. Western blot analysis on the specific CK2 phosphorylation targets: (a) phosphorylation of the Akt1 serine 129 and (b) Cdc37 serine 13 in HCT-116 cells inoculated with varying levels of **1c** (5, 10, and 20 μM) for 24 h.

example, **1c** exhibited potent antiproliferative activities against five different CK2-overexpressed cancer cells, especially PC-3 cells and HCT-116 cells with IC_{50} values of 4.53 and 3.07 μM, respectively. **1i** showed considerable potency against MCF-7 cells (4.51 μM) and HT-29 cells (3.52 μM); more importantly, it was less toxic to LO2 with an IC_{50} value higher than 200 μM. In addition, **1m** showed a more potent activity against PC-3 cells, and the IC_{50} value is 3.28 μM. However, compounds **1m**, **1p**, **1q**, **2f**, and **2g** with lower CK2 inhibitory activities than **CX-4945**, probably because of their steric hindrances or long methylene chains, had less antiproliferation activities against cancer cells than **CX-4945**. It was also worth noting that compounds **1j** and **1k** with moderate CK2 inhibitory activities also exhibited strong anticancer activity. When ester bonding served as the linker, the resulting compounds (**2a**−**e**) demonstrated much better cytotoxicity than **CX-4945**. In particular, **2c** not only displayed potent activity against CK2 but also showed strong inhibitory influence toward five different cancer cells. However, it was a little toxic to normal liver cells LO2. The possible reason is that functional groups varied from carboxylic acid to amide or ester in **CX-4945** might change the pharmacokinetic properties and the antitumor and CK2 inhibitory activity of the resulting compounds. Based on the above study, **1c** with high selectivity for CK2, potent inhibitory activity against the tested cancer cells, low toxicity to normal liver cells, and a suitable LLE value was chosen for further investigation.

Investigation of the Representative Compound on Its CK2α Targeting. To confirm that **1c** can act directly on endogenous CK2α as well, the phosphorylation level of Akt1 serine 129 (p-Akt1^{S129}) and Cdc37 serine 13 (p-Cdc37^{S13}), the two specific phosphorylation targets of CK2, was also investigated by western blot in HCT-116 cells. As shown in Figure 4a,b, compound **1c** can obviously suppress the expression of p-Akt1^{S129} and p-Cdc37^{S13} in a dose-dependent manner, suggesting that **1c** can not only inhibit exogenous CK2α but also inhibit endogenous CK2α in HCT-116 cells.

In addition, molecular docking simulations of **1c** with CK2α and Clk2 were also performed using AutoDock Vina. CK2α (PDB ID: 6isj) and Clk2 (PDB ID: 6khe) co-structures complexed with **CX-4945** were used as a template. As shown in Figure 5a, compound **1c** is bound tightly to the surface of

https://doi.org/10.1021/acs.jmedchem.1c00131
J. Med. Chem. 2021, 64, 5082−5098

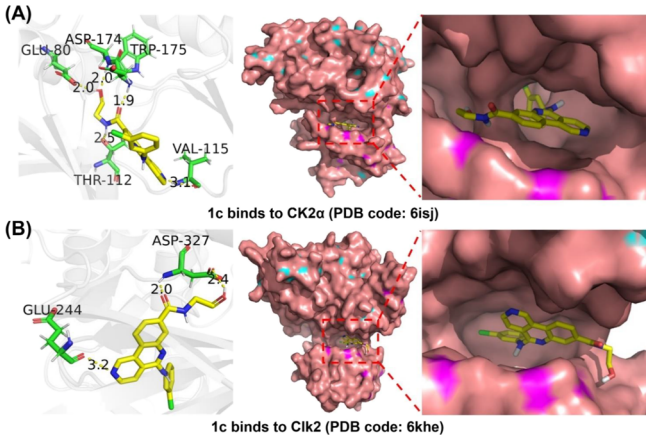

Figure 5. Molecular docking. Docking of **1c** into (a) CK2α (PDB ID: 6isj) and (b) Clk2 (PDB ID: 6khe) kinase X-ray crystal structure. Potentially relevant residues to the docking are labeled. Interactions are illustrated by dashed lines (H bonds, yellow).

the protein with good compatibility. The amide serving as both a hydrogen bond donor and a hydrogen bond acceptor forms two important hydrogen bonds with TRP-175 and THR-112 residues *via* its O and H atom, respectively. The N atom on the ring A of naphthyridine produces a hydrogen bond with the VAL-115 residue. Meanwhile, the hydroxyl group on the side chain of 2-aminoethanol also forms hydrogen bonding with ASP-174 and GLU-80 residues by its O and H atom, respectively. The five hydrogen bonds enable the entire **1c** skeleton to be firmly anchored deep in the CK2α active cavity. Compared with CK2α, **1c** is not inserted deep into the activity cavity of Clk2 (Figure 5b). There are only three hydrogen bonds between **1c** and the amino acid residues in the active cavity of Clk2. The hydrogen atoms from the amide and the hydroxyl group generate hydrogen bonding with ASP-127 residues, respectively, while the N atom in ring A has hydrogen bonds with GLU-224 residues. The results illustrate that **1c** binds CK2α more tightly than Clk2.

Investigation on the Inhibition of ALDH1A1. It has been proven that CK2α positively modulates Notch1 transcriptional activity and the population of $CD44^+/CD24^-$, which participate in stem cell maintenance.[31] With the inherent CK2 inhibitory activity, we hypothesize that **1c** may also inhibit cancer cell stemness by regulating stem-cell-related signaling pathways. As aldehyde dehydrogenase 1-A1 (ALDH1A1), one of the strongest CSC hallmarks, plays a core role in sustaining the stemness of HCT-116 cells,[32] it was detected to quantify the proportion of $ALDH^+$ cells. As shown in Figure 6a (see also Supporting Information Figure S1), the ratio of the $ALDH^+$ cell subpopulation was up to 63% in HCT-116 cells, indicating that **1c** could strongly inhibit the proportion of intracellular $ALDH^+$ cell subsets and present a concentration-dependent inhibitory manner. The inhibitory ratio of **1c** reached 96% at 20 μM and 77% even at 5 μM, significantly higher than that of **CX-4945** (61%) at the same concentration of 5 μM. This was further validated by the related western blotting analysis (Figure 6a). Moreover, the impact of **1c** on ALDH1A1 expression in HCT-116 cells was investigated. As expected, the transcriptional level of ALDH1A1 in HCT-116 cells decreased significantly after being treated with **1c** (20 μM) for 24 h, which was only half of that in the **CX-4945**-treated group (Figure 6c). In addition, we also evaluated the inhibitory activity of **1c** against the exogenous ALDH1A1 enzyme. As shown in Figure 6d, both **CX-4945** and **1c** can inhibit exogenous ALDH1A1 enzyme activity in a dose-dependent manner, especially **1c**, with an IC_{50} value of 0.10 μM that is 8.8 times higher than that of **CX-4945**. To further elucidate the binding mechanism between **1c**

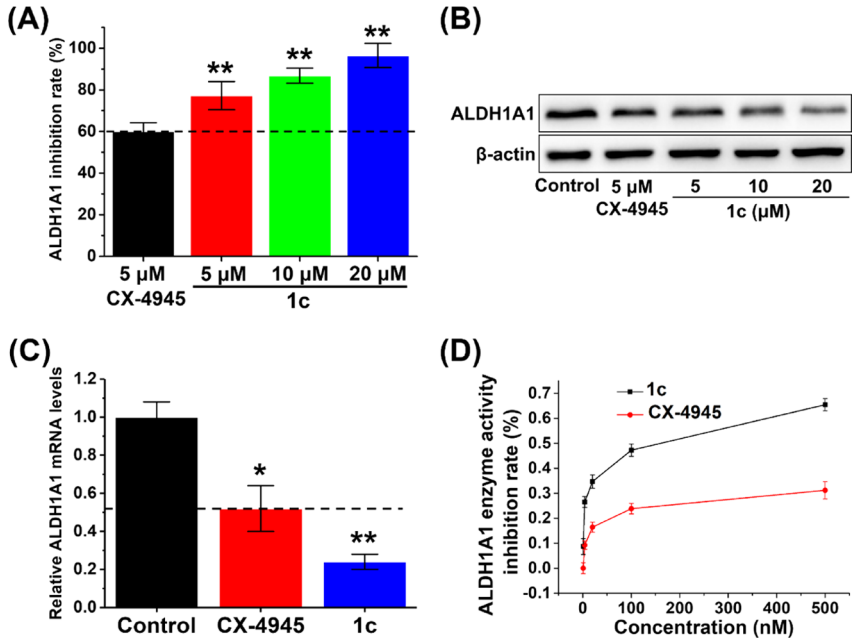

Figure 6. Investigation on the inhibition of **1c** on ALDH1A1. (a) A statistical analysis of the ALDH1A1 inhibitory ratio. (b) Western blotting assessment on expression of ALDH1A1 protein in HCT-116 cells treated with **CX-4945** (5 μM) and different quantities of **1c** (5, 10, and 20 μM) for 24 h, respectively. (c) mRNA transcription levels of ALDH1A1 after exposure to **CX-4945** and **1c** at 20 μM, respectively, in the HCT-116 cells for 24 h. (d) Inhibition rate of **1c** and **CX-4945** at different concentrations on the enzyme activity of ALDH1A1. Data were subjected to statistical analysis by using Student's *t* test and given as the mean ± SD (n = 3). *P < 0.05 and **P < 0.01 vs **CX-4945** group or the control group.

https://doi.org/10.1021/acs.jmedchem.1c00131
J. Med. Chem. 2021, 64, 5082−5098

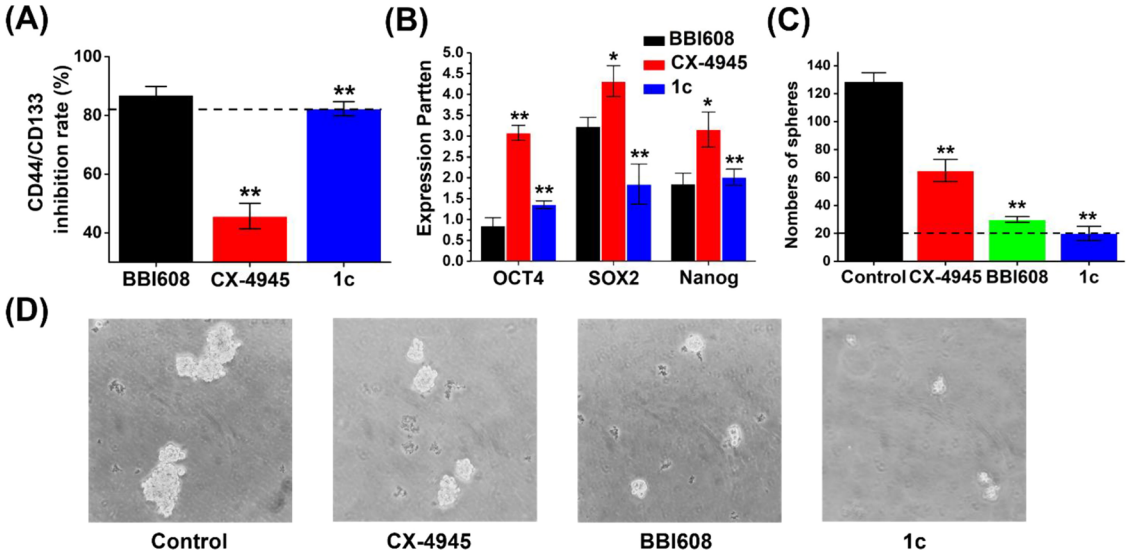

Figure 7. Investigation on the inhibition of cancer cell stemness. (a) A statistical analysis of the $CD44^+/CD133^+$ inhibitory ratio. (b) qRT-PCR of mRNA transcription levels of stemness genes after exposure to **BBI608**, **CX-4945**, and **1c**, respectively, at 20 μM in the HCT-116^{ALDH+} cells for 24 h. (c) The number and (d) the morphological observation of the HCT-116^{AHDH+} cell tumorspheres treated with vehicle (DMSO), **BBI608** (5 μM), **CX-4945** (5 μM), and **1c** (5 μM) for 24 h and then cultivated for 10 days. Comparison of gene expression level was performed using the $2^{-\Delta\Delta Ct}$ approach. Data were subjected to statistical analysis by using Student's *t* test and given as the mean ± SD ($n = 3$). $^*P < 0.05$ and $^{**}P < 0.01$ vs **BBI608** group or the control group.

and ALDH1A1, we performed a related molecular docking study. As shown in Figure S2, the N atom in ring A, O atom in amide, and OH group in 2-aminoethanol form hydrogen bonding with GLY-458, CYS-303, and ASN-170 residues, respectively. These hydrogen bonds hold **1c** firmly in the ALDH1A1 active cavity. These results demonstrate that **1c** can target ALDH1A1 protein and inhibit its activity, and regulate certain signaling pathways to inhibit the transcription and protein expression of ALDH1A1.

Investigation on the Inhibition of Cancer Cell Stemness. Based on the inhibitory effect of **1c** on ALDH1A1, we further explored the influence of **1c** on the stemness driven by ALDH in HCT-116 cells. $ALDH^+$ population cells in HCT-116 cells were sorted by flow cytometer and named HCT-116^{ALDH+} cells. It is known that CSC surface antigens' expression is cancer type-distinct or cancer subtype-distinct. Since they play a vital role in invasiveness and promoting cancer recurrence, it is pivotal to comprehend how CSCs are modulated and maintained at the molecular level.[22] To examine the influence of **1c** on the cancer cell stemness, the expression of $CD44^+$ and $CD133^+$ in HCT-116^{ALDH+} cells treated with **1c** was determined by flow cytometry using **CX-4945** and napabucasin (**BBI608**) as the positive controls. **BBI608**, currently in Phase II/III clinical trials, is a known STAT3 inhibitor that can potently block spherogenesis, kill stem cancer cells isolated from numerous kinds of cancer, and repress stemness gene expression.[33] As shown in Figure 7a and Figure S3, compound **1c** shows a potent inhibitory effect on $CD44^+/CD133^+$, with an inhibitory rate of about 84%, second only to **BBI608** (89%), which is 1.45 times higher than that of **CX-4945** (58%). SOX2, OCT4, and Nanog, essential transcription factors to maintain the characteristics of stem cells, are currently recognized as the signature genes of CSCs, which have an important role in maintaining self-renewal along with proliferation in malignant tumors.[34] The influence of **1c** on the transcription levels of the signature genes of CSCs in HCT-116^{ALDH+} cells was quantitatively analyzed. As shown in Figure 7b, noticeable differences in mRNA expression were observed for the transcription factor. **CX-4945** had the weakest inhibitory activity, whose transcription levels of OCT4, SOX2, and Nanog were 2.27, 2.34, and 1.57 times as many as those of **1c**, respectively. It is noteworthy that the level of SOX2 transcription in HCT-116^{ALDH+} cells treated with **BBI608** was 1.75 times higher than the **1c** group despite the transcription levels of OCT4 and Nanog being slightly lower than the **1c** group. It has been documented that the high expression level of SOX2 enhances the tumorigenic potential by regulating the expressions of genes that participate in proliferation, apoptosis, and cell cycle modulation.[35] In addition, SOX2 overexpressed in human colon CSCs promotes chemotherapy resistance and tumor growth. The capability of tumorsphere formation was also tested. As shown in Figure 7c,d, obvious phenotypic alterations were observed in HCT-116^{ALDH+}-derived tumorspheres in all the groups. HCT-116^{ALDH+} cells treated with **1c** exhibited fewer sphere number and smaller size than those treated with either **CX-4945** or **BBI608**. This also proved that **1c** has a stronger inhibitory effect on the cancer cell stemness than **BBI608**.

Investigation on the Signaling Pathway of Wnt/β-Catenin. The Wnt/β-catenin signaling pathway plays a core role in tumor invasion, especially in tumor metastasis and differentiation.[36,37] β-Catenin binds to the TCF/LEF transcription factor family in the nucleus to activate the promoter of β-catenin target genes, thus activating the target genes of the Wnt signaling pathway like CD44, CD24, CD133, ABCG2, ALDH1A1, EpCAM, MMP7, Vimentin, and Slug. It has been confirmed that Wnt1 can enhance ALDH1A1 expression, hence enhancing the expression of Akt as well as β-catenin.[38] Phosphorylated Akt inactivates GSK-3β through phosphorylating GSK-3β at ser9, repressing its capacity to degrade β-catenin.[39,40] Therefore, it is suggested that **1c** might regulate the expression of ALDH1A1 through the Akt-GSK-3β(ser9)-Wnt/β-catenin signaling pathway, thereby affecting tumor

https://doi.org/10.1021/acs.jmedchem.1c00131
J. Med. Chem. 2021, 64, 5082−5098

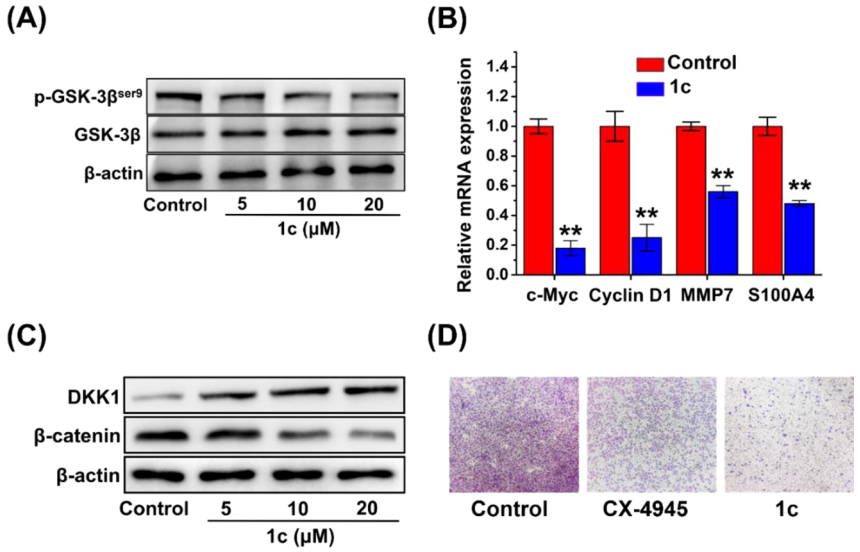

Figure 8. Compound **1c** regulated the GSK-3β(ser9)-Wnt/β-catenin signaling pathway. Western blotting images of (a) p-GSK-3β(ser9), GSK-3β, (c) DKK1, and β-catenin proteins induced by different concentrations of **1c** for 24 h in HCT-116 cells. (b) Decreased mRNA levels of Wnt target genes in HCT-116 cells upon exposure to **1c** (20 μM) for 24 h. (d) Transwell invasion assays. The HCT-116 cells were inoculated with **1c** and **CX-4945**, respectively, at 5 μM for 24 h. Data were subjected to statistical analysis by using Student's *t* test and given as the mean ± SD (n = 3). *P < 0.05 and **P < 0.01 vs the control group.

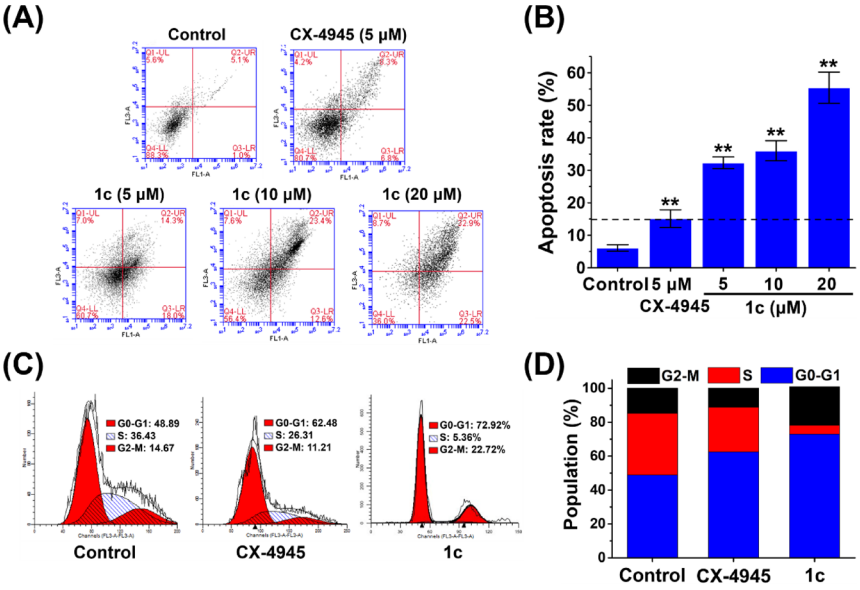

Figure 9. Cell apoptosis and cell cycle arrest analysis. (a) Cell apoptosis in HCT-116 cells treated with **CX-4945** (5 μM) and varying levels of **1c** (5, 10, and 20 μM) was assessed using flow cytometry (stained with Annexin V-FITC and PI). (b) A statistical analysis of apoptotic ratio. (c) Cell cycle arrest in HCT-116 cells inoculated with **CX-4945** (20 μM) and **1c** (20 μM), respectively, for 24 h; stained with PI; and explored with flow cytometry. (d) A statistical analysis of cell cycle arrest. The results were given as the mean ± SD (n = 3). **P < 0.01 vs the control group.

invasion and metastasis. As illustrated in Figure 8a, compound **1c** significantly inhibited GSK-3β(ser9) protein phosphorylation in HCT-116 cells dose-dependently. In addition, the mRNA levels of Wnt target genes consisting of c-Myc, cyclin D1, MMP7, and S100A4 were remarkably reduced upon treatment of **1c** (Figure 8b). Meanwhile, the protein level of DKK1 was upregulated with the increasing concentrations of **1c**, while that of β-catenin was significantly downregulated (Figure 8c). In addition, **1c** also exhibited a superior capacity to repress the invasion of HCT-116 cells (Figure 8d). The above results indicated that **1c** decreased the activity of CK2 by specifically targeting CK2 and then reduced ALDH1A1 expression and inhibited the invasion of cancer cells by suppressing the Akt1(ser129)-GSK-3β(ser9)-Wnt/β-catenin signaling pathway.

Investigation on the Cell Apoptosis and Cell Cycle Arrest. Cell apoptosis was measured *via* flow cytometric assays. HCT-116 cells after being treated with **CX-4945** (5 μM) and varying levels of **1c** (5, 10, and 20 μM) for 24 h were analyzed. As shown in Figure 9a,b, at the same concentration (5 μM), the ratio of apoptosis triggered by **1c** was much higher in contrast with that of **CX-4945**. With the increasing concentration, the proportion of apoptosis induced by **1c** also increased gradually. At the concentration of 20 μM, the apoptotic ratio reached about 55%, exhibiting a dose-dependent behavior. The effect of **1c** on HCT-116 cell cycle

https://doi.org/10.1021/acs.jmedchem.1c00131
J. Med. Chem. 2021, 64, 5082−5098

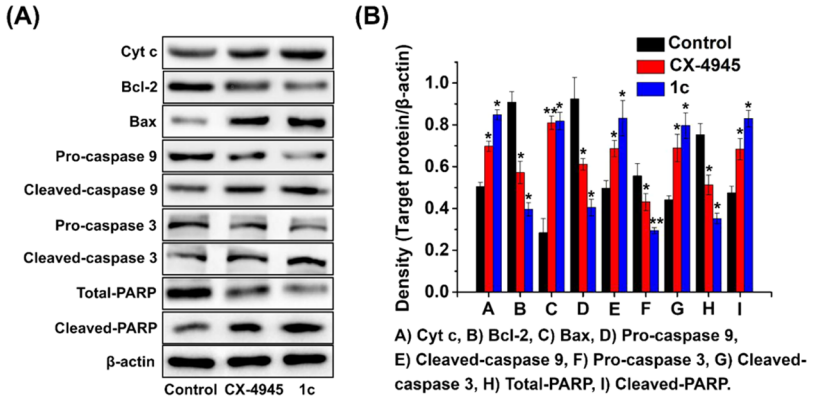

Figure 10. Study on the mechanism of apoptotic pathway. (a) Western blotting assessment of Cyt c, Bcl-2, Bax, pro-caspase 9, cleaved caspase 9, pro-caspase 3, cleaved caspase 3, total PARP, cleaved PARP as well as β-actin after 24 h treatment of HCT-116 cells with **CX-4945** (20 μM) and **1c** (20 μM), respectively. (b) Expression levels of (a) acquired from western blotting and standardized with β-actin. The results are given as the mean ± SD (n = 3). $^{**}P < 0.01$ and $^{*}P < 0.05$ vs the control group.

progression was examined *via* flow cytometry, with **CX-4945** serving as the positive control. Due to the analogous structure, both **CX-4945** and **1c** arrested the cell cycle at the G0−G1 phase in HCT-116 cells as illustrated in Figure 9c,d.

Investigation on the Mechanism of Apoptotic Pathway. The mitochondrial linked apoptotic proteins including cytochrome c (Cyt c), Bax, Bcl-2, pro-caspase 9, cleaved caspase 9, pro-caspase 3, cleaved caspase 3, total PARP, and cleaved PARP were assessed in HCT-116 cells after inoculation with **1c** by western blotting, using **CX-4945** as the positive control. The results are indicated in Figure 10a,b. In contrast with the control, **1c** induced an obvious decrease in the level of Bcl-2 and increased the Bax expression to a higher degree than **CX-4945**. Moreover, treatment of **1c** in HCT-116 cells released more Cyt c than that of **CX-4945**, resulting in the activation of the downstream caspase cascade. The activations of downstream caspases and PARP were observed, which were able to trigger the apoptosis of cancer cells. As expected, exposure of HCT-116 cells to **1c** caused more starkly downregulation in the levels of pro-caspase 9, pro-caspase 3, and total PARP and upregulation in the levels of cleaved caspase 9, cleaved caspase 3, and cleaved PARP relative to **CX-4945**. These results indicate that **1c** can induce HCT-116 cell apoptosis through a mitochondrial-mediated signaling pathway and caspase cascade.

Pharmacokinetic Study. The pharmacokinetic profiles of **1c** and **CX-4945** were evaluated in Sprague−Dawley (SD) rats following a single 25 mg/kg dose administration by the oral route. To be consistent with previous reports,[29] **CX-4945** was transformed into its sodium salt (**CX-4945·Na**). As summarized in Table 3, the PK profile of **1c** is similar to that of **CX-4945·Na** with a slight improvement. The maximal drug concentration (C_{max}) reached 7017.8 ng/mL in plasma, elimination half-life ($t_{1/2}$) was approximately 6.67 h, and the plasma exposure AUC_{0-t} and $AUC_{0-\infty}$ were above 4000 ng·h/mL, which were a little better than those of **CX-4945·Na** except for the clearance. These results reveal that **1c** presents a favorable pharmacokinetic behavior.

***In Vivo* Antitumor Activity.** The antitumor activity of **1c** in HCT-116 xenograft models was tested, in which animals were grouped randomly into four groups as vehicle, **CX-4945·Na** (60 mg/kg), and **1c** at two doses (60 and 90 mg/kg) and administrated po twice a day for 4 weeks. The volume of tumors and body weight were assessed every 3 days. As illustrated in Figure 11a−c, the inhibitory rate (59%) of **1c** at the low dose is 3.9 times higher than that (15%) of **CX-4945·Na**. In addition, it is noticed that **1c** obviously inhibits the tumor growth dose-dependently with a maximum inhibitory rate of 69% at a dose of 90 mg/kg. There is no conspicuous change in body weight of all the mice treated with **1c**. Furthermore, the HE staining of slices from the heart, liver, spleen, lung, and kidney of an animal randomly selected from each tested group in HCT-116 models demonstrates that **1c** at the used dosages has hardly toxic effects on organ tissues (Figure S4), revealing that **1c** has low systemic toxicity and good safety (Figure 11d). These results indicate that **1c** exhibits potent antitumor activity with low toxicity in the HCT-116 xenograft mice model.

Table 3. Pharmacokinetic Parameters of Compound 1c in SD Rats[a]

parameter	CX-4945·Na	1c
T_{max} (h)	2.00 ± 0.00	2.33 ± 0.58
C_{max} (ng·mL^{-1})	6786.32 ± 223.88	7017.81 ± 297.85
$t_{1/2}$ (h)	5.82 ± 0.27	6.67 ± 1.59
CL (L·h^{-1}·kg^{-1})	0.63 ± 0.01	0.60 ± 0.03
AUC_{0-t} (ng·h·mL^{-1})	38,919.58 ± 90.48	40,460.61 ± 2353.48
$AUC_{0-\infty}$ (ng·h·mL^{-1})	39,994.05 ± 74.29	41,450.07 ± 2378.31
V_d (L·kg^{-1})	2.39 ± 0.50	2.77 ± 0.25
MRT_{0-t} (h)	6.45 ± 0.55	6.21 ± 0.26
$MRT_{0-\infty}$ (h)	6.52 ± 0.61	6.26 ± 0.29

[a] T_{max}, time for peak concentration; C_{max}, peak value; $t_{1/2}$, elimination half-life period; CL, plasma clearance; AUC, area under the time concentration curve; V_d, apparent volume of distribution; and MRT, mean residue time.

CONCLUSIONS

Herein, a series of 5-(3-chlorophenylamino)benzo[*c*][2,6]-naphthyridine derivatives were synthesized with **CX-4945** as the lead compound. **1c** stands out for its excellent selectivity and inhibitory activity on CK2. Biological studies indicated that **1c** exhibited stronger CK2 inhibitory activity with much higher ClK2/CK2 selectivity than **CX-4945**, which greatly reduces the off-target toxicity of **CX-4945**. In addition, **1c** also exhibited a potent inhibitory effect on cancer cell stemness. Further research on the mechanism of action reveals that **1c** can inhibit the Akt1(ser129)-GSK-3β(ser9)-Wnt/β-catenin

https://doi.org/10.1021/acs.jmedchem.1c00131
J. Med. Chem. 2021, 64, 5082−5098

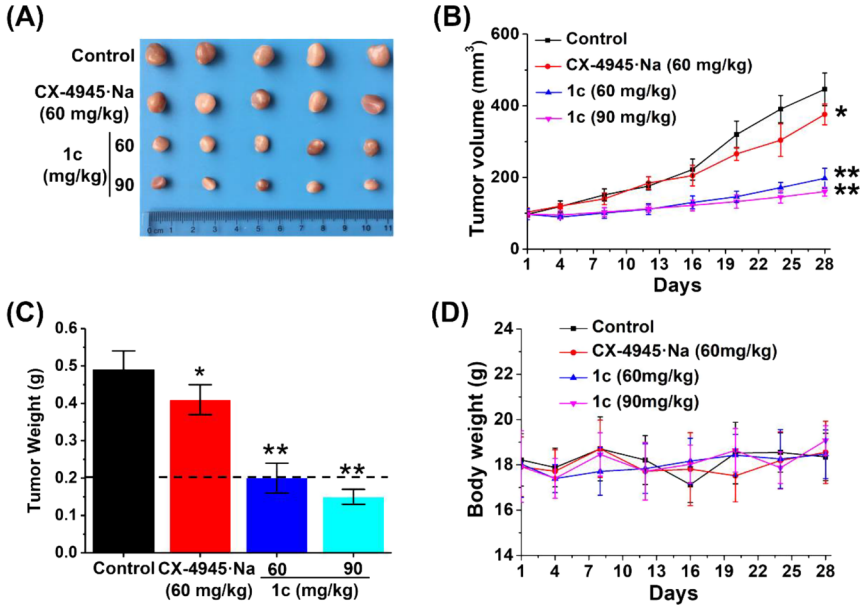

Figure 11. *In vivo* HCT-116 xenograft model study of **1c**. Twenty nude mice inoculated with HCT-116 cells in the right armpit were divided into four groups as vehicle (equivalent volume of CMC-Na), **CX-4945·Na** (60 mg/kg), and **1c** (60 and 90 mg/kg). Animals were orally administrated twice a day for 4 weeks. (a) Excised tumor images from each group. (b) The relative volume of the tumors. (c) The relative tumor weight resected from all groups of sacrificed mice on the last day. (d) The body weights of each group mice in the period of 28 days. Data are given as the mean ± SD. $^*P < 0.05$ and $^{**}P < 0.01$ vs the control group.

signaling pathway and inhibit the expression of the stemness markers ALDH1A1, CSCs surface antigens ($CD44^+$ and $CD133^+$), and stem genes (SOX2, OCT4, and Nanog), thereby inhibiting the CSCs. Furthermore, **1c** displayed superior pharmacokinetics and antitumor activity compared with **CX-4945·Na** without obvious toxicity. The development of novel antitumor drugs and therapeutic strategies targeting the CK2 and CSCs in tumors is a still unmet need, but it may represent a definite advantage in cancer treatment. The identification of **1c** is a step forward in this direction. The favorable antiproliferative and antitumor activities of **1c** make it possible for **1c** to act as a multifunctional drug candidate to suppress CK2 protein and CSCs for the treatment of cancer.

EXPERIMENTAL SECTION

Materials and Instruments. All chemical reagents along with the solvents were commercially acquired from Energy Chemical, Acros, Alfa, Maybridge, or Adamas-beta and utilized without further purification. Flash column chromatography employed a silica gel (100−200 mesh). NMR spectra were obtained in DMSO-d_6, unless otherwise stated, on Bruker 600 (^{1}H at 600 MHz, ^{13}C at 150 MHz) NMR spectrometers, and tetramethylsilane (TMS) was employed as reference. An Agilent 6224 ESI/TOF MS instrument was employed to measure the mass spectra. Purities of the tested compounds, determined by RP-HPLC analysis using a Waters e2965 HPLC with ODS column (5 μm, 250 × 4.6 mm column and methanol/water), were ≥ 95%. All cell lines utilized herein were purchased from Biorn Lifescience Co., Ltd. (Nanjiang, Jiangsu, China). p-Akt1^{S129}, Akt, p-Cdc37^{S13}, Cdc37, p-GSK-3β(ser9), GSK-3β, DKK1, β-catenin, Cyt c, Bax, Bcl-2, pro-caspase 9, cleaved caspase 9, pro-caspase 3, cleaved caspase 3, total PARP, cleaved PARP, and β-actin antibodies were supplied by Beyotime Biotechnology. The HRP-conjugated secondary antibody (1: 2000) was provided by Santa Cruz Biotechnologies.

Synthesis and Characterization of the Compounds. Compound **BTE** and **CX-4945** were synthesized following the previously documented procedures[29] and verified by ^{1}H NMR. Compound **BTE**: ^{1}H NMR (600 MHz, DMSO-d_6) δ 10.09 (s, 1H), 9.91 (s, 1H), 8.94 (d, J = 5.6 Hz, 1H), 8.79 (d, J = 8.5 Hz, 1H), 8.77 (d, J = 5.6 Hz, 1H), 8.34 (t, J = 1.9 Hz, 1H), 8.17 (dd, J = 6.3, 1.4 Hz, 2H), 7.90 (dd, J = 8.4, 1.7 Hz, 1H), 7.42 (t, J = 8.1 Hz, 1H), 7.12 (dd, J = 7.9, 1.4 Hz, 1H), 3.92 (s, 3H) ppm; **CX-4945**: ^{1}H NMR (600 MHz, DMSO-d_6) δ12.04 (s, 1H), 10.30 (s, 1H), 10.16(s, 1H), 9.08 (d, J = 5.8 Hz, 1H), 9.00−8.97 (m, 1H), 8.94 (d, J = 8.5 Hz, 1H), 8.31−8.28 (m, 2H), 8.12 (d, J = 8.2 Hz, 1H), 8.03 (dd, J = 8.4, 1.5 Hz, 1H), 7.45 (t, J = 8.1 Hz, 1H), 7.17 (d, J = 7.9 Hz, 1H) ppm.

Synthesis of ***1a.*** KOH (1.12 g, 20 mmol) and $NH_2OH·HCl$ (0.695 g, 10 mmol) were dissolved in 5 and 8 mL MeOH, respectively, to get solutions A and B. Then, solution A was added dropwise to solution B at 0 °C. The temperature of the reaction system was slowly raised to room temperature, and the reaction was continued for 30 min. At the end of the reaction, the precipitated solid was removed by suction filtration to obtain an alkaline hydroxylamine solution. **BTE** (0.36 g, 1 mmol) was dissolved in alkaline hydroxylamine solution (5 mL), stirred 1 h at room temperature, and monitored by TLC. After the substrate was completely consumed, the solvent was removed under vacuum, and the residue was acidified with 2 M HCl to pH = 5−6, filtering the precipitate; washed with H_2O (3 × 15 mL); and dried to obtain the crude product of **1b**. The precipitate was recrystallized with MeOH (10 mL) to get a bright yellow solid (0.332 g). Yield: 91.2%. ^{1}H NMR (600 MHz, DMSO-d_6) δ 11.52 (s, 1H), 10.16 (s, 1H), 9.65 (s, 1H), 9.19 (s, 1H), 8.97 (d, J = 5.4 Hz, 1H), 8.83 (d, J = 8.4 Hz, 1H), 8.57 (d, J = 5.2 Hz, 1H), 8.33 (s, 1H), 8.15 (d, J = 1.2 Hz, 1H), 8.07 (d, J = 8.0 Hz, 1H), 7.85 (d, J = 1.2 Hz, 1H), 7.43 (t, J = 8.0 Hz, 1H), 7.13 (dd, J = 7.8, 1.2 Hz, 1H) ppm. ^{13}C NMR (150 MHz, DMSO-d_6) δ 164.19, 150.52, 148.13, 147.73, 143.74, 142.35, 134.16, 133.27, 130.53, 127.49, 126.08, 124.19, 122.95, 122.90, 122.64, 121.54, 120.60, 119.60, 116.81 ppm. HR-MS (m/z) (ESI): calcd for $C_{19}H_{13}ClN_4O_2$ $[M + H]^+$: 365.0805; found: 365.0800.

General Procedure for Preparation of Compounds ***1b−1o.*** *5-((3-Chlorophenyl)amino)-N-(methylsulfonyl)benzo[c][2,6]-naphthyridine-8-carboxamide (****1b****).* To a solution of **CX-4945** (0.210 g, 0.6 mmol) in *N*,*N*-dimethylformamide (DMF) (5 mL) was added 2-(7-azabenzotriazol-1-yl)-*N*,*N*,*N*′,*N*′-tetramethyluronium hexafluorophosphate (HATU) (0.273 g, 0.72 mmol) and stirred at room temperature for 10 min. Then, *N*,*N*-diisopropylethylamine (DIPEA) (0.197 mL, 1.2 mmol) was added to the solution and stirred for 10 min at the same temperature, followed by addition of methanesulfonamide (0.048 g, 0.5 mmol), and the solution was stirred overnight in

https://doi.org/10.1021/acs.jmedchem.1c00131
J. Med. Chem. 2021, 64, 5082−5098

a nitrogen atmosphere. The progress of the reaction was monitored with TLC. After the substrate was completely consumed, the solvent was removed under vacuum, and the residue was treated with EtOAc (50 mL). The organic layers were washed with saturated salt water (3 × 20 mL) and dried with anhydrous Na_2SO_4. The organic layers were concentrated under vacuum to obtain the crude product and further purified with silica gel chromatography with the eluent of MeOH and DCM (1:100−1:50) to give a yellow solid **1b** (0.093 g). Yield: 43.5%. ^{1}H NMR (600 MHz, DMSO-d_6) δ 13.26 (s, 1H), 10.19 (s, 1H), 9.69 (s, 1H), 9.01 (d, J = 5.5 Hz, 1H), 8.87 (d, J = 8.4 Hz, 1H), 8.60 (d, J = 5.6 Hz, 1H), 8.33 (s, 1H), 8.28 (s, 1H), 8.10 (d, J = 8.2 Hz, 1H), 7.99 (d, J = 8.1 Hz, 1H), 7.45 (t, J = 8.1 Hz, 1H), 7.16−7.13 (d, J = 7.8 Hz, 1H), 2.51 (s, 3H) ppm. ^{13}C NMR (150 MHz, DMSO-d_6) δ 150.71, 150.60, 148.30, 148.09, 143.76, 142.33, 133.24, 130.62, 128.72, 127.42, 124.70, 124.47, 123.13, 123.08, 122.80, 122.67, 120.57, 119.61, 116.86, 63.26 ppm. HR-MS (m/z) (ESI): calcd for $C_{20}H_{15}ClN_4O_3S$ $[M + H]^+$: 427.0631; found: 427.0643.

*5-((3-Chlorophenyl)amino)-N-(2-hydroxyethyl)benzo[c][2,6]-naphthyridine-8-carboxamide (**1c**).* Yellow solid. Yield: 72.1%. ^{1}H NMR (600 MHz, DMSO-d_6) δ 10.18 (s, 1H), 9.89 (s, 1H), 8.97 (d, J = 5.4 Hz, 1H), 8.84 (t, J = 6.0 Hz, 2H), 8.77 (d, J = 5.4 Hz, 1H), 8.35 (s, 1H), 8.27 (s, 1H), 8.21 (d, J = 8.2 Hz, 1H), 8.00 (d, J = 8.2 Hz, 1H), 7.45 (t, J = 8.0 Hz, 1H), 7.14 (d, J = 7.6 Hz, 1H), 4.91 (t, J = 5.6 Hz, 1H), 3.61 (q, J = 5.8 Hz, 2H), 3.43 (dd, J = 11.2, 5.4 Hz, 2H) ppm. ^{13}C NMR (150 MHz, DMSO-d_6) δ 166.40, 150.61, 148.05, 147.64, 143.77, 142.51, 135.92, 133.19, 130.46, 127.52, 126.40, 124.25, 123.38, 122.71, 122.56, 121.46, 120.70, 119.73, 117.16, 60.20, 42.88 ppm. HR-MS (m/z) (ESI): calcd for $C_{21}H_{17}ClN_4O_2$ $[M + H]^+$: 393.1118; found: 393.1120.

*N-(2-Aminoethyl)-5-((3-chlorophenyl)amino)benzo[c][2,6]-naphthyridine-8-carboxamide (**1d**).* Yellow solid. Yield: 81.6%. Compound **1d** may also be prepared by the method reported in the literature.[41] ^{1}H NMR (600 MHz, DMSO-d_6) δ 10.12 (s, 1H), 9.60 (s, 1H), 8.95 (d, J = 5.4 Hz, 1H), 8.81−8.79 (m, 1H), 8.54 (s, 1H), 8.53 (d, J = 5.6 Hz, 1H), 8.24 (t, J = 1.8 Hz, 1H), 8.20 (d, J = 1.4 Hz, 1H), 8.09 (d, J = 8.2 Hz, 1H), 7.93 (dd, J = 8.2, 1.4 Hz, 1H), 7.42 (t, J = 8.2 Hz, 1H), 7.11 (d, J = 7.8 Hz, 1H), 3.45 (dd, J = 12.6, 6.4 Hz, 2H), 3.35 (m, 2H), 1.94−1.88 (m, 2H) ppm. ^{13}C NMR (150 MHz, DMSO-d_6) δ 166.29, 150.46, 148.07, 147.66, 143.75, 142.37, 135.96, 133.26, 130.52, 127.48, 126.25, 124.13, 123.30, 122.74, 122.62, 121.45, 120.65, 119.65, 116.78, 37.98, 29.60 ppm. HR-MS (m/z) (ESI): calcd for $C_{21}H_{18}ClN_5O$ $[M + H]^+$: 393.1278; found: 393.1280.

*N-(2-Bromoethyl)-5-((3-chlorophenyl)amino)benzo[c][2,6]-naphthyridine-8-carboxamide (**1e**).* Yellow solid. Yield: 61.4%. ^{1}H NMR (600 MHz, DMSO-d_6) δ 10.20 (s, 1H), 9.67 (s, 1H), 9.12 (t, J = 5.0 Hz, 1H), 9.00 (d, J = 5.4 Hz, 1H), 8.82 (d, J = 3.8 Hz, 1H), 8.59 (d, J = 5.4 Hz, 1H), 8.29 (s, 1H), 8.28 (s, 1H), 8.13 (d, J = 8.0 Hz, 1H), 7.97 (d, J = 8.2 Hz, 1H), 7.45 (t, J = 8.0 Hz, 1H), 7.15 (d, J = 7.6 Hz, 1H), 4.85 (t, J = 5.2 Hz, 2H), 3.88−3.84 (m, 2H) ppm.^{13}C NMR (150 MHz, DMSO-d_6) δ 166.69, 152.29, 150.61, 148.16, 147.77, 143.79, 142.37, 135.05, 133.28, 130.55, 127.50, 126.41, 124.25, 123.36, 122.87, 122.71, 120.76, 119.76, 116.84, 79.74, 38.61 ppm. HR-MS (m/z) (ESI): calcd for $C_{21}H_{16}BrClN_4O$ $[M + H]^+$: 455.0274; found: 455.0272.

*5-((3-Chlorophenyl)amino)-N-(2,2-difluoroethyl)benzo[c][2,6]-naphthyridine-8-carboxamide (**1f**).* Yellow solid. Yield: 61.8%. ^{1}H NMR (600 MHz, DMSO-d_6) δ 10.18 (s, 1H), 9.99 (s, 1H), 9.28 (s, 1H), 8.96 (d, J = 4.6 Hz, 1H), 8.86 (d, J = 8.2 Hz, 1H), 8.83 (d, J = 4.6 Hz, 1H), 8.37 (s, 1H), 8.29 (s, 1H), 8.22 (d, J = 7.4 Hz, 1H), 8.01 (d, J = 7.8 Hz, 1H), 7.44 (t, J = 7.8 Hz, 1H), 7.14 (d, J = 7.2 Hz, 1H), 6.23 (t, J = 13.2 Hz, 1H), 3.77 (t, J = 14.8 Hz, 2H) ppm. ^{13}C NMR (150 MHz, DMSO-d_6) δ 166.98, 150.76, 148.05, 147.77, 143.80, 142.50, 134.89, 133.17, 130.42, 127.44, 126.57, 124.37, 123.31, 122.90, 122.59, 121.87, 120.80, 119.82, 117.29, 115.09 (t, J = 240.2 Hz), 42.25 (t, J = 26.6 Hz) ppm. HR-MS (m/z) (ESI): calcd for $C_{21}H_{15}ClF_2N_4O$ $[M + H]^+$: 413.0980; found: 413.0967.

*5-((3-Chlorophenyl)amino)-N-(2-(dimethylamino)ethyl)benzo-[c][2,6]naphthyridine-8-carboxamide (**1g**).* Yellow solid. Yield: 69.8%. ^{1}H NMR (600 MHz, DMSO-d_6) δ 10.18 (s, 1H), 9.67 (s, 1H), 8.98 (d, J = 5.6 Hz, 1H), 8.84 (d, J = 8.4 Hz, 1H), 8.72 (t, J = 5.4 Hz, 1H), 8.59 (d, J = 5.6 Hz, 1H), 8.28 (t, J = 1.8 Hz, 1H), 8.23 (d, J = 1.4 Hz, 1H), 8.11 (dd, J = 8.4, 1.0 Hz, 1H), 7.94 (dd, J = 8.4, 1.6 Hz, 1H), 7.45 (t, J = 8.2 Hz, 1H), 7.15 (dd, J = 7.8, 1.4 Hz, 1H), 3.45 (dd, J = 12.8, 6.6 Hz, 2H), 2.53−2.51 (m, 2H), 2.25 (s, 6H) ppm. ^{13}C NMR (150 MHz, DMSO-d_6) δ 166.19, 150.54, 148.13, 147.70, 143.77, 142.39, 135.94, 133.27, 130.54, 127.53, 126.29, 124.20, 123.35, 122.76, 122.66, 121.50, 120.71, 119.70, 116.83, 58.59, 45.64, 37.92 ppm. HR-MS (m/z) (ESI): calcd for $C_{23}H_{22}ClN_5O$ $[M + H]^+$: 420.1591; found: 420.1595.

*5-((3-Chlorophenyl)amino)-N-(prop-2-yn-1-yl)benzo[c][2,6]-naphthyridine-8-carboxamide (**1h**).* Yellow solid. Yield: 76.4%. ^{1}H NMR (600 MHz, DMSO-d_6) δ 10.17 (s, 1H), 9.96 (s, 1H), 9.36 (t, J = 5.2 Hz, 1H), 8.96 (d, J = 5.4 Hz, 1H), 8.85 (d, J = 8.4 Hz, 1H), 8.82 (d, J = 5.5 Hz, 1H), 8.40 (s, 1H), 8.28 (s, 1H), 8.23 (d, J = 8.2 Hz, 1H), 8.00 (d, J = 8.3 Hz, 1H), 7.45 (t, J = 8.1 Hz, 1H), 7.15 (d, J = 7.8 Hz, 1H), 4.18 (d, J = 3.2 Hz, 2H), 3.21 (s, 1H) ppm. ^{13}C NMR (1500 MHz, DMSO-d_6) δ 166.06, 150.67, 147.69, 143.78, 142.50, 135.11, 133.17, 130.40, 128.23, 127.42, 126.52, 124.31, 123.26, 122.83, 122.54, 121.73, 120.71, 119.74, 117.23, 81.83, 73.37, 29.12 ppm. HR-MS (m/z) (ESI): calcd for $C_{22}H_{15}ClN_4O$ $[M + H]^+$: 387.1012; found: 387.1011.

*Methyl 3-(5-((3-Chlorophenyl)amino)benzo[c][2,6]-naphthyridine-8-carboxamido)propanoate (**1i**).* Yellow solid. Yield: 65.4%. ^{1}H NMR (600 MHz, DMSO-d_6) δ 10.18 (s, 1H), 9.66 (s, 1H), 8.99 (d, J = 5.6 Hz, 1H), 8.88 (t, J = 5.4 Hz, 1H), 8.85 (d, J = 8.4 Hz, 1H), 8.58 (d, J = 5.6 Hz, 1H), 8.28 (t, J = 1.8 Hz, 1H), 8.22 (d, J = 1.4 Hz, 1H), 8.10 (dd, J = 8.2, 1.2 Hz, 1H), 7.93 (dd, J = 8.4, 1.6 Hz, 1H), 7.45 (t, J = 8.2 Hz, 1H), 7.15 (dd, J = 7.8, 1.2 Hz, 1H), 3.65 (s, 3H), 3.58 (dd, J = 12.6, 6.8 Hz, 2H), 2.68 (t, J = 7.0 Hz, 2H) ppm. ^{13}C NMR (150 MHz, DMSO-d_6) δ 172.28, 166.39, 150.55, 148.15, 147.73, 143.76, 142.37, 135.72, 133.27, 130.55, 127.51, 126.31, 124.21, 123.33, 122.81, 122.68, 121.58, 120.71, 119.71, 116.82, 51.89, 36.13, 34.02 ppm. HR-MS (m/z) (ESI): calcd for $C_{23}H_{19}ClN_4O_3$ $[M + H]^+$: 435.1224; found: 435.1220.

*5-((3-Chlorophenyl)amino)-N-(2-(pyrrolidin-1-yl)ethyl)benzo[c]-[2,6]naphthyridine-8-carboxamide (**1j**).* Yellow solid. Yield: 72.8%. ^{1}H NMR (600 MHz, DMSO-d_6) δ 10.19 (s, 1H), 9.69 (s, 1H), 9.00 (d, J = 5.6 Hz, 1H), 8.97 (d, J = 5.2 Hz, 1H), 8.88 (d, J = 8.4 Hz, 1H), 8.58 (d, J = 5.6 Hz, 1H), 8.26 (d, J = 4.2 Hz, 2H), 8.05 (d, J = 8.0 Hz, 1H), 7.96 (d, J = 8.2 Hz, 1H), 7.44 (t, J = 8.2 Hz, 1H), 7.16 (d, J = 7.8 Hz, 1H), 3.66 (dd, J = 10.8, 4.8 Hz, 2H), 3.37 (m, 6H), 1.96 (m, 4H) ppm. ^{13}C NMR (150 MHz, DMSO-d_6) δ 166.99, 150.73, 148.20, 147.90, 143.79, 142.32, 135.29, 133.29, 130.59, 127.49, 126.43, 124.32, 123.43, 122.92, 122.83, 121.85, 120.90, 119.89, 116.88, 54.06, 53.91, 36.50, 23.00 ppm. HR-MS (m/z) (ESI): calcd for $C_{25}H_{24}ClN_5O$ $[M + H]^+$: 446.1747; found: 446.1750.

*5-((3-Chlorophenyl)amino)-N-(2-(piperidin-1-yl)ethyl)benzo[c]-[2,6]naphthyridine-8-carboxamide (**1k**).* Yellow solid. Yield: 77.1%. ^{1}H NMR (600 MHz, DMSO-d_6) δ 10.19 (s, 1H), 9.69 (s, 1H), 9.00 (d, J = 5.4 Hz, 2H), 8.88 (d, J = 8.4 Hz, 1H), 8.59 (d, J = 5.6 Hz, 1H), 8.27 (s, 1H), 8.25 (d, J = 0.8 Hz, 1H), 8.05 (d, J = 8.2 Hz, 1H), 7.96 (dd, J = 8.4, 1.0 Hz, 1H), 7.45 (t, J = 8.2 Hz, 1H), 7.16 (dd, J = 7.8, 1.2 Hz, 1H), 3.70 (dd, J = 11.8, 5.8 Hz, 2H), 3.59 (t, J = 5.8 Hz, 2H), 3.30 (t, J = 6.2 Hz, 2H), 2.97 (t, J = 6.4 Hz, 2H), 1.91−1.61 (m, 6H) ppm. ^{13}C NMR (150 MHz, DMSO-d_6) δ 167.00, 151.59, 148.20, 147.90, 143.79, 142.31, 135.24, 133.28, 130.59, 129.32, 126.43, 124.32, 123.39, 122.96, 122.83, 121.19, 120.89, 119.88, 116.88, 55.62, 52.81, 34.77, 22.99, 21.68 ppm. HR-MS (m/z) (ESI): calcd for $C_{26}H_{26}ClN_5O$ $[M + H]^+$: 460.1904; found: 460.1900.

*5-((3-Chlorophenyl)amino)-N-(2-morpholinoethyl)benzo[c][2,6]-naphthyridine-8-carboxamide (**1l**).* Yellow solid. Yield: 68.7%. Compound **1l** may also be prepared by the method reported in the literature.[41] ^{1}H NMR (600 MHz, DMSO-d_6) δ 10.16 (s, 1H), 9.98 (s, 1H), 8.94 (d, J = 5.6 Hz, 1H), 8.84 (d, J = 5.2 Hz, 2H), 8.82 (s, 1H), 8.38 (s, 1H), 8.22 (s, 1H), 8.19 (d, J = 8.3 Hz, 1H), 7.96 (d, J = 8.2 Hz, 1H), 7.42 (t, J = 8.1 Hz, 1H), 7.12 (dd, J = 7.8, 0.9 Hz, 1H), 3.62 (m, 4H), 3.49 (m, 2H), 3.38 (m, 4H), 2.61 (m, 2H) ppm. ^{13}C NMR (150 MHz, DMSO-d_6) δ 166.30, 150.71, 148.04, 147.67, 143.80, 142.56, 135.89, 133.16, 130.42, 127.53, 126.36, 124.31, 123.32,

https://doi.org/10.1021/acs.jmedchem.1c00131
J. Med. Chem. 2021, 64, 5082−5098

122.79, 122.55, 121.53, 120.79, 119.81, 117.37, 66.36, 63.29, 57.60, 53.54 ppm. HR-MS (m/z) (ESI): calcd for $C_{25}H_{24}ClN_5O_2$ $[M + H]^+$: 462.1697; found: 462.1695.

*5-((3-Chlorophenyl)amino)-N-(3-hydroxypropyl)benzo[c][2,6]-naphthyridine-8-carboxamide (**1m**).* Yellow solid. Yield: 79.8%. ^{1}H NMR (600 MHz, DMSO-d_6) δ 10.19 (s, 1H), 9.67 (s, 1H), 8.99 (d, J = 5.6 Hz, 1H), 8.85 (d, J = 8.4 Hz, 1H), 8.77 (t, J = 5.6 Hz, 1H), 8.59 (d, J = 5.6 Hz, 1H), 8.28 (s, 1H), 8.23 (s, 1H), 8.12 (dd, J = 8.2, 1.0 Hz, 1H), 7.95 (dd, J = 8.4, 1.6 Hz, 1H), 7.45 (t, J = 8.2 Hz, 1H), 7.15 (dd, J = 7.8, 1.2 Hz, 1H), 4.54 (t, J = 5.2 Hz, 1H), 3.52 (q, J = 6.2 Hz, 2H), 3.40 (dd, J = 12.8, 7.0 Hz, 2H), 1.75 (p, J = 6.6 Hz, 2H) ppm. ^{13}C NMR (150 MHz, DMSO-d_6) δ 166.27, 150.53, 148.15, 147.70, 143.78, 142.39, 136.06, 133.27, 130.56, 127.54, 126.27, 124.19, 123.35, 122.77, 122.66, 121.46, 120.68, 119.69, 116.84, 59.13, 37.22, 32.92 ppm.HR-MS (m/z) (ESI): calcd for $C_{22}H_{19}ClN_4O_2$ $[M + H]^+$: 407.1269; found: 407.1264.

*N-(3-Aminopropyl)-5-((3-chlorophenyl)amino)benzo[c][2,6]-naphthyridine-8-carboxamide (**1n**).* Yellow solid. Yield: 57.3%. ^{1}H NMR (600 MHz, DMSO-d_6) δ 10.19 (s, 1H), 10.01 (s, 1H), 8.96 (d, J = 5.6 Hz, 1H), 8.91 (t, J = 5.4 Hz, 1H), 8.87 (d, J = 3.8 Hz, 1H), 8.38 (s, 1H), 8.25−8.21 (m, 2H), 8.04 (s, 1H), 7.99 (d, J = 8.4 Hz, 1H), 7.44 (t, J = 8.2 Hz, 1H), 7.14 (d, J = 7.8 Hz, 1H), 3.36 (dd, J = 12.6, 6.4 Hz, 2H), 3.18 (dd, J = 12.8, 6.2 Hz, 2H), 1.76−1.70 (m, 2H), 1.22 (s, 2H) ppm. ^{13}C NMR (150 MHz, DMSO-d_6) δ 166.25, 161.58, 150.71, 148.07, 147.68, 143.82, 142.56, 135.91, 133.16, 130.46, 127.55, 126.34, 124.30, 123.21, 122.79, 122.56, 120.77, 119.82, 117.38, 37.53, 35.51, 29.61 ppm. HR-MS (m/z) (ESI): calcd for $C_{22}H_{20}ClN_5O$ $[M + H]^+$: 406.1434; found: 406.1431.

*Methyl 4-(5-((3-Chlorophenyl)amino)benzo[c][2,6]-naphthyridine-8-carboxamido)butanoate (**1o**).* Orange solid. Yield: 65.8%. ^{1}H NMR (600 MHz, DMSO-d_6) δ 10.17 (s, 1H), 9.94 (s, 1H), 8.95 (d, J = 6.0 Hz, 1H), 8.87−8.83 (m, 2H), 8.81 (d, J = 5.0 Hz, 1H), 8.34 (s, 1H), 8.22 (s, 1H), 8.19 (d, J = 8.0 Hz, 1H), 7.95 (d, J = 7.8 Hz, 1H), 7.43 (t, J = 7.8 Hz, 1H), 7.13 (d, J = 7.4 Hz, 1H), 3.59 (s, 3H), 3.35 (dd, J = 12.6, 6.8 Hz, 2H), 2.41 (t, J = 6.8 Hz, 2H), 1.87−1.81 (m, 2H) ppm. ^{13}C NMR (150 MHz, DMSO-d_6) δ 173.68, 166.36, 150.69, 148.03, 147.66, 143.79, 142.52, 135.91, 133.17, 130.46, 127.54, 126.30, 124.29, 123.35, 122.76, 122.59, 121.49, 120.78, 119.81, 117.30, 51.75, 39.15, 31.36, 24.94 ppm. HR-MS (m/z) (ESI): calcd for $C_{24}H_{21c}lN_4O_3$ $[M + H]^+$: 449.1380; found: 449.1386.

*General Procedure for Preparation of Compounds **1p**−**1q**. 3-(5-((3-Chlorophenyl)amino)benzo[c][2,6]naphthyridine-8-carboxamido)propanoic Acid (**1p**).* General procedure B: To a solution of **1i** (0.434 g, 1 mmol) in MeOH (10 mL) were added H_2O (5 mL) and LiOH·H_2O (0.105 g, 2.5 mmol) and stirred at 60 °C overnight. The progress of the reaction was monitored with TLC. After the substrate was completely consumed, the solvent was removed under vacuum, and the residue was acidified with 1 M HCl to pH = 5, filtering the precipitate; washed with water (3 × 10 mL); and dried to obtain the crude product of **1p**. The crude product was recrystallized with MeOH (15 mL) to get a yellow solid (0.370 g). Yield: 88.1%. ^{1}H NMR (600 MHz, DMSO-d_6) δ 12.37 (s, 1H), 10.15 (s, 1H), 9.63 (s, 1H), 8.96 (s, 1H), 8.84 (s, 1H), 8.81 (d, J = 7.4 Hz, 1H), 8.55 (s, 1H), 8.24 (t, J = 1.8 Hz, 1H), 8.21 (d, J = 1.2 Hz, 1H), 8.09 (d, J = 6.8 Hz, 1H), 7.92 (dd, J = 7.2, 1.8 Hz, 1H), 7.42 (d, J = 6.8 Hz, 1H), 7.13 (d, J = 6.4 Hz, 1H), 3.54 (dd, J = 10.6, 5.8 Hz, 2H), 2.58 (t, J = 6.4 Hz, 2H) ppm. ^{13}C NMR (150 MHz, DMSO-d_6) δ 173.63, 166.29, 150.52, 148.12, 147.69, 143.75, 142.37, 135.77, 133.27, 130.54, 127.50, 126.30, 124.18, 123.32, 122.76, 122.65, 121.53, 120.68, 119.68, 116.80, 36.31, 34.40 ppm. HR-MS (m/z) (ESI): calcd for $C_{22}H_{17}ClN_4O_3$ $[M + H]^+$: 421.1067; found: 421.1060.

*4-(5-((3-Chlorophenyl)amino)benzo[c][2,6]naphthyridine-8-carboxamido)butanoic Acid (**1q**).* Yellow solid. Yield: 83.6%. ^{1}H NMR (600 MHz, DMSO-d_6) δ 12.43 (s, 1H), 10.18 (s, 1H), 9.66 (d, J = 5.3 Hz, 1H), 8.99 (d, J = 5.4 Hz, 1H), 8.84 (d, J = 8.4 Hz, 1H), 8.81 (t, J = 6.4 Hz, 1H), 8.58 (d, J = 5.4 Hz, 1H), 8.27 (s, 1H), 8.24 (s, 1H), 8.13 (d, J = 8.5 Hz, 1H), 7.96 (d, J = 8.3 Hz, 1H), 7.46 (t, J = 8.1 Hz, 1H), 7.15 (d, J = 7.5 Hz, 1H), 3.38 (dd, J = 12.6, 6.5 Hz, 2H), 2.35 (t, J = 7.3 Hz, 2H), 1.87−1.81 (m, 2H) ppm. ^{13}C NMR (150 MHz, DMSO-d_6) δ 174.80, 166.28, 150.50, 148.13, 147.68, 143.76, 142.38, 135.96, 133.27, 130.55, 127.52, 126.30, 124.17, 123.37, 122.74, 122.64, 121.47, 120.67, 119.67, 116.81, 39.29, 31.72, 25.05 ppm. HR-MS (m/z) (ESI): calcd for $C_{23}H_{19}ClN_4O_3$ $[M + H]^+$: 435.1224; found: 435.1221.

*General Procedure for Preparation of Compounds **2a**−**2g**. 2-Hydroxyethyl 5-((3-Chlorophenyl)amino)benzo[c][2,6]-naphthyridine-8-carboxylate (**2a**).* General procedure C: To a solution of **CX-4945** (0.210 g, 0.6 mmol) in DMF (5 mL) was added *O*-(benzotriazol-1-yl)-*N*,*N*,*N*′,*N*′-tetramethyluronium tetrafluoroborate (TBTU) (0.231 g, 0.72 mmol) and stirred at 45 °C for 10 min. Then, triethylamine (TEA) (0.167 mL, 1.2 mmol) was added to the solution and stirred for 10 min at the same temperature, followed by the addition of ethylene glycol (0.062 g, 1 mmol), and the solution was stirred for 24 h in a nitrogen atmosphere. The progress of the reaction was monitored with TLC. After the substrate was completely consumed, the solvent was removed under vacuum, and the residue was treated with EtOAc (25 mL). The organic layers were washed with saturated salt water (3 × 20 mL) and dried with anhydrous Na_2SO_4. The organic layers were concentrated under vacuum to obtain the crude product and further purified with silica gel chromatography with the eluent of MeOH and DCM (1:100−1:50) to give a yellow solid (0.204 g). Yield: 86.5%. ^{1}H NMR (600 MHz, DMSO-d_6)δ 10.17 (s, 1H), 9.95 (s, 1H), 8.99 (d, J = 5.6 Hz, 1H), 8.88 (d, J = 8.5 Hz, 1H), 8.79 (d, J = 5.6 Hz, 1H), 8.32 (t, J = 2.0 Hz, 1H), 8.27 (d, J = 1.6 Hz, 1H), 8.18 (dd, J = 8.2, 1.3 Hz, 1H), 8.01 (dd, J = 8.4, 1.7 Hz, 1H), 7.45 (t, J = 8.1 Hz, 1H), 7.15 (dd, J = 7.9, 1.4 Hz, 1H), 5.12 (t, J = 5.4 Hz, 1H), 4.39−4.35 (m, 2H), 3.78 (dd, J = 9.4, 4.8 Hz, 2H) ppm. ^{13}C NMR (150 MHz, DMSO-d_6) ^{13}C NMR (151 MHz, DMSO) δ 166.18, 150.85, 148.21, 148.16, 143.76, 142.34, 133.15, 131.11, 130.52, 128.59, 127.27, 124.62, 124.41, 123.23, 123.15, 122.71, 120.79, 119.85, 117.26, 67.36, 59.52 ppm. HR-MS (m/z) (ESI): calcd for $C_{21}H_{16}ClN_3O_3$ $[M + H]^+$: 394.0958; found: 394.0961.

*2-Iodoethyl 5-((3-Chlorophenyl)amino)benzo[c][2,6]-naphthyridine-8-carboxylate (**2b**).* Yellow solid. Yield: 77.3%. ^{1}H NMR (600 MHz, DMSO-d_6) δ 10.16 (s, 1H), 10.04 (s, 1H), 8.98 (d, J = 5.6 Hz, 1H), 8.82 (d, J = 8.5 Hz, 1H), 8.52 (dd, J = 8.3, 1.0 Hz, 1H), 8.34 (s, 1H), 8.26 (d, J = 8.2 Hz, 1H), 8.02 (d, J = 1.4 Hz, 1H), 7.73 (dd, J = 8.4, 1.5 Hz, 1H), 7.48 (t, J = 8.1 Hz, 1H), 7.16 (dd, J = 7.9, 1.2 Hz, 1H), 5.11−5.08 (t, J = 8.2 Hz, 2H), 4.78 (t, J = 7.8 Hz, 2H). ^{13}C NMR (150 MHz, DMSO-d_6) δ 165.62, 152.34, 150.89, 148.19, 143.68, 142.39, 133.15, 130.50, 130.26, 128.49, 127.20, 124.66, 124.04, 123.26, 123.17, 122.71, 120.89, 119.95, 117.39, 79.06, 63.61. HR-MS (m/z) (ESI): calcd for $C_{21}H_{15}ClF_2N_4O$ $[M + H]^+$: 503.9975; found: 503.9980.

*2-Fluoroethyl 5-((3-Chlorophenyl)amino)benzo[c][2,6]-naphthyridine-8-carboxylate (**2c**).* Yellow solid. Yield: 82.8%. ^{1}H NMR (600 MHz, DMSO-d_6) δ 10.11 (s, 1H), 9.64 (s, 1H), 8.97 (d, J = 5.4 Hz, 1H), 8.82 (d, J = 8.2 Hz, 1H), 8.54 (d, J = 5.2 Hz, 1H), 8.22 (s, 1H), 8.20 (s, 1H), 8.07 (d, J = 8.0 Hz, 1H), 7.94 (d, J = 8.2 Hz, 1H), 7.44 (t, J = 8.0 Hz, 1H), 7.14 (dd, J = 7.8, 1.2 Hz, 1H), 4.88−4.86 (m, 1H), 4.80−4.77 (m, 1H), 4.65−4.62 (m, 1H), 4.59−4.57 (m, 1H) ppm. ^{13}C NMR (150 MHz, DMSO-d_6) δ 165.79, 150.59, 148.15, 148.11, 143.62, 142.15, 133.19, 130.51, 130.46, 128.53, 127.08, 124.44, 124.18, 123.20, 123.18, 122.70, 120.64, 119.64, 116.72, 82.22 (d, J = 166.2 Hz), 64.72 (d, J = 18.2 Hz) ppm. HR-MS (m/z) (ESI): calcd for $C_{21}H_{15}ClFN_3O_2$ $[M + H]^+$: 396.0915; found: 396.0911.

*2-(Pyridin-2-yl)ethyl 5-((3-Chlorophenyl)amino)benzo[c][2,6]-naphthyridine-8-carboxylate (**2d**).* Yellow solid. Yield: 77.2%. ^{1}H NMR (600 MHz, DMSO-d_6) δ 10.15 (s, 1H), 10.02 (s, 1H), 8.97 (s, 1H), 8.87 (d, J = 7.0 Hz, 1H), 8.83 (s, 1H), 8.61 (s, 1H), 8.36 (s, 1H), 8.27 (s, 1H), 8.18 (d, J = 6.1 Hz, 1H), 8.00 (d, J = 6.7 Hz, 1H), 7.88 (s, 1H), 7.57 (d, J = 5.3 Hz, 1H), 7.43 (s, 1H), 7.39 (s, 1H), 7.13 (d, J = 5.9 Hz, 1H), 5.50 (s, 2H), 3.40 (s, 1H), 3.18 (s, 1H) ppm. ^{13}C NMR (150 MHz, DMSO-d_6) δ 165.78, 156.03, 150.96, 149.74, 148.25, 143.82, 142.36, 137.58, 133.11, 130.64, 130.47, 128.69, 127.23, 124.71, 124.32, 123.63, 123.44, 122.68, 122.50, 122.10,

https://doi.org/10.1021/acs.jmedchem.1c00131
J. Med. Chem. 2021, 64, 5082−5098

120.83, 119.88, 118.27, 117.41, 67.41, 49.03 ppm. HR-MS (m/z) (ESI): calcd for $C_{26}H_{19}ClN_4O_2$ $[M + H]^+$: 455.1275; found: 455.1269.

*2,2-Difluoroethyl 5-((3-Chlorophenyl)amino)benzo[c][2,6]-naphthyridine-8-carboxylate (**2e**).* Earth-yellow solid. Yield: 65.7%. ^{1}H NMR (600 MHz, DMSO-d_6) δ 10.10 (s, 1H), 9.90 (s, 1H), 8.96 (d, J = 5.6 Hz, 1H), 8.83 (d, J = 8.5 Hz, 1H), 8.76 (d, J = 5.4 Hz, 1H), 8.31 (d, J = 1.7 Hz, 1H), 8.19 (d, J = 1.7 Hz, 1H), 8.16−8.14 (m, 1H), 7.93 (dd, J = 8.4, 1.8 Hz, 1H), 7.44 (t, J = 8.2 Hz, 1H), 7.14 (dd, J = 7.8, 1.2 Hz, 1H), 6.51 (tt, J = 54.2, 3.2 Hz, 1H), 4.68 (td, J = 15.2, 3.2 Hz, 2H) ppm. ^{13}C NMR (150 MHz, DMSO-d_6) δ 165.21, 150.86, 148.21, 148.12, 143.70, 142.25, 133.12, 130.41, 129.78, 128.69, 127.07, 124.63, 124.17, 123.51, 123.37, 122.69, 120.82, 119.82, 117.19, 114.12 (t, J = 238.9 Hz), 63.04 (t, J = 26.4 Hz).HR-MS (m/z) (ESI): calcd for $C_{21}H_{14}ClF_2N_3O_2$ $[M + H]^+$: 414.0821; found: 414.0820.

*3,3-Dichloropropyl 5-((3-Chlorophenyl)amino)benzo[c][2,6]-naphthyridine-8-carboxylate (**2f**).* Yellow solid (0.141 g). Yield: 61.5%. ^{1}H NMR (600 MHz, DMSO-d_6) δ 10.14 (s, 1H), 10.02 (s, 1H), 8.97 (d, J = 5.6 Hz, 1H), 8.87 (d, J = 3.6 Hz, 1H), 8.86 (s, 1H), 8.39 (t, J = 1.8 Hz, 1H), 8.24 (d, J = 1.4 Hz, 1H), 8.17 (dd, J = 8.2, 1.2 Hz, 1H), 7.98 (dd, J = 8.4, 1.6 Hz, 1H), 7.43 (t, J = 8.2 Hz, 1H), 7.14 (dd, J = 7.8, 1.2 Hz, 1H), 4.84−4.80 (m, 1H), 4.70 (dd, J = 11.8, 4.6 Hz, 1H), 4.65 (dd, J = 11.8, 6.2 Hz, 1H), 4.14 (t, J = 5.2 Hz, 2H) ppm. ^{13}C NMR (150 MHz, DMSO-d_6) δ 165.47, 150.91, 148.21, 148.17, 143.75, 142.34, 133.12, 130.40, 130.23, 128.72, 127.17, 124.67, 124.27, 123.44, 123.36, 122.67, 120.86, 119.87, 117.38, 65.77, 58.78, 46.48 ppm. HR-MS (m/z) (ESI): calcd for $C_{22}H_{16}Cl_3N_3O_2$ $[M + H]^+$: 460.0386; found: 460.0380.

*2-(2-(2-Hydroxyethoxy)ethoxy)ethyl 5-((3-Chlorophenyl)amino)-benzo[c][2,6]naphthyridine-8-carboxylate (**2g**).* Yellow solid. Yield: 72.6%. ^{1}H NMR (600 MHz, DMSO-d_6) δ 10.12 (s,1H), 9.63 (s, 1H), 8.98 (d, J = 6.0 Hz, 1H), 8.82 (d, J = 6.0 Hz, 1H), 8.54 (d, J = 6.0 Hz, 1H), 8.27 (t, J = 2.0 Hz, 1H), 8.20 (d, J = 1.6 Hz, 1H), 8.07 (dd, J = 8.2, 1.4 Hz, 1H), 7.94 (dd, J = 8.4, 1.8 Hz, 1H), 7.45 (t, J = 8.1 Hz, 1H), 7.15 (dd, J = 6.0, 1.4 Hz, 1H), 4.57 (t, J = 6.0 Hz, 1H), 4.47 (t, J = 6.0 Hz, 2H), 3.83 (t, J = 6.0 Hz, 2H), 3.66 (dd, J = 5.8, 3.8 Hz, 2H), 3.58 (dd, J = 5.8, 3.8 Hz, 2H), 3.48 (dd, J = 10.4, 4.8 Hz,2H), 3.44 (dd, J = 7.8, 3.0 Hz, 2H) ppm. ^{13}C NMR (150 MHz, DMSO-d_6) δ 165.97, 150.65, 148.22, 148.16, 143.67, 142.19, 133.22, 130.88, 130.54, 128.53, 127.19, 124.49, 124.25, 123.21, 123.15, 122.73, 120.67, 119.67, 116.78, 72.86, 70.41, 70.27, 68.84, 64.79, 60.69 ppm. HR-MS (m/z) (ESI): calcd for $C_{25}H_{24}ClN_3O_5$ $[M + H]^+$: 482.1482; found: 482.1483.

CK2, ClK2, and ALDH1A1 Assay. CK2, Clk2, and the ALDH1A1 Kinase (Human) Assay/Inhibitor Screening Assay Kit as well as CK2, Clk2, and ALDH1A1 enzymes were supplied by Shanghai Fusheng Industrial Co., Ltd. (Shanghai, China). The inhibitory activity of tested compounds on CK2, ClK2, and ALDH1A1 was detected according to manufacturer's instruction by commercial CK2, ClK2, and ALDH1A1 assay kits with **CX-4945** as the positive control. As shown in Figure S7, we take CK2 enzyme activity detection as an example to briefly introduce the experimental process. 50 μL, 60 U/L of CK2 enzyme reaction solution was added to each well of 96-well plates after thawing, and then five gradient concentrations (500.0, 100.0, 20.0, 4.0, and 0.8 nM) of fresh compound solutions were added to each well, respectively. In addition, the same solution without the inhibitor was added to each well in the control group. The 96 well plate was sealed with sealing film and incubated in 37 °C incubator for 2 h. After that, the conjugate reagent (50 μL) was introduced to every well, except for the control group, and incubated at 37 °C for another 30 min. The color developing reagents A (50 μL) and B (50 μL) were successively added to each hole, the mixture was shaken gently and mixed well, light was avoided for 15 min, and then the stop buffer (50 μL) was added to each hole. The reaction mixtures were incubated at room temperature for 10 min, and the value of O.D. was measured *via* an enzyme-labeling instrument at 450 nm. The IC_{50} value of each compound is given as the mean ± SD and was obtained by three parallel experiments.

Cell Line Culture. The CK2-overexpressed cell lines PC-3 (prostate cancer cell line), HCT-116 (colorectal cancer cell line), MCF-7 (breast cancer cell line), HT-29 (colorectal cancer cell line), and T24 (bladder Cancer Cell line) and the normal human liver cell line LO2 were grown under 5% CO_2 and 95% air at 37 °C conditions. All these cells were grown in monolayer in DMEM or RPMI-1640 medium enriched with 10% FBS, 100 μg/mL streptomycin, and 100 μg/mL penicillin solutions.

Antiproliferative Assay. MTT assay was used to detect the antiproliferative effect of all the target compounds against several cancer cell lines. About 5 × 10^3 cells per well were planted in a 96-well plate and incubated at 37 °C in 5% CO_2 overnight. Compounds were dissolved with DMSO and diluted with medium to various concentrations, and added to these different cells culture medium, respectively, for 72 h. After that, 10 μL of 5 mg/mL MTT was introduced to all the wells, and incubation of the cells was continued for 4 h. The medium was discarded, and 150 μL of DMSO was added to dissolve the dark blue crystals on the bottom. The value of O.D. was determined with an enzyme-labeling instrument at 490 nm. The IC_{50} value of each compound presented as the mean ± SD was obtained by three parallel experiments.

Kinase Inhibition Assays. The potential of compound **1c** as a CK2 inhibitor was determined at 1 μmol/L concentration against a panel of 208 kinases through the commercially available service provided by ICE Bioscience Inc. (Beijing, China).

Molecular Docking. Molecular docking of **1c** to CK2α (PDB ID: 6isj), Clk2 (PDB ID: 6khe), and ALDH1A1 (PDB ID: 4x4l) was conducted *via* AutoDock Vina, where the Iterated Local Search Globule Optimizer was employed as the optimization algorithm. Ligand **1c** was prepared in ChemBioDraw Ultra 14.0 and minimized with ChemBio3D Ultra 14.0. Before the docking process, the natural ligand along with the water molecules was deleted from the crystal structure. Subsequently, all hydrogen atoms were added to the each protein and ligand to be docked, and every coordinate file of the protein, as well as the ligand was generated as a PDBQT file *via* AutoDockTools-1.5.6. A grid box for binding site covered the protein's catalytic site. The box possessed a 1.0 Å grid spacing and was centered at the geometric center of the protein. In every docking experiment, we selected the best binding mode on the basis of the binding affinity determined by the scoring function in AutoDock Vina. Docking results were analyzed and visualized with PyMOL (Schroedinger LLC, NY).

ALDH Activity Assay. The HCT-116 cells were inoculated on six-well plates at 2 × 10^5 cells per well; grown at 37 °C in 5% CO_2 overnight; and then treated with **CX-4945** (5 μM), different concentrations of **1c** (5, 10, and 20 μM), and vehicle (DMSO), respectively, for 24 h, to explore ALDH1A1 expression in HCT-116 cells. Aldefluor (Stem Cell Technologies, Vancouver, BC, Canada) staining was assayed with the FITC channel of fluorescent activated cell sorting as described by the manufacturer. To mark the base fluorescence, pretreatment with the DEAB ALDH inhibitor was employed as a negative control to mark the base fluorescence.

Quantitative Real-Time PCR Assay. TRIZOL was employed to isolate total cellular RNA from HCT-116 or HCT-116^{ALDH+} cells treated for 24 h with the tested compounds. RNA was reverse-transcribed with the Luna universal one-step RT-qPCR (GeneAmp 9600, PERKIN ELMER), and the resulting cDNA was subsequently run on a thermal cycler (ABI StepOnePlus, ABI). Thermal profile was as follows: reverse transcription for 10 min at 55 °C and initial denaturation for 1 min at 95 °C followed by 39 thermal cycles of denaturation for 10 s at 95 °C and extension for 30 s at 60 °C. Primer sequences are listed in Table S1. All PCRs included melting curve analysis and template-free negative technical controls to verify specific single-product amplification. β-Actin mRNA was employed as an internal standard. The relative expression of mRNA is represented as fold increase ($2^{-\Delta\Delta Ct}$).[42]

CD44 and CD133 Expression Assay. The HCT-116^{ALDH+} cells were planted in six-well plates at 2 × 10^5 cells per well; cultured overnight under 37 °C and 5% CO_2 conditions; and then treated with vehicle (DMSO), **BBI608** (20 μM), **CX-4945** (20 μM), and **1c** (20

https://doi.org/10.1021/acs.jmedchem.1c00131
J. Med. Chem. 2021, 64, 5082−5098

μM), respectively. After co-incubation for 24 h, we collected the cells and stained them with PE-labeled anti-CD133 and FITC-labeled anti-CD44 for 30 min as described by the manufacturer. The expression of $CD44^+$ along with $CD133^+$ was detected with flow cytometry by the Cell Quest software.

Cancer Stem-like Spheroid Formation Assay. A spheroid formation assay was used to explore the stemness of HCT-116^{ALDH+} cells. Concisely, 800 cells/well were planted in the 24-well plates (3473, Corning) in serum-free DMEM enriched with B27 (17504044, Invitrogen, 1: 50), EGF (20 ng/mL, AF-100-15, Peprotech), and β-FGF (10 ng/mL, 100-18B, Peprotech). Vehicle (DMSO), **BBI608** (5 μM), **CX-4945** (5 μm) along with 1C (5 μm) were added into each well of the 24-well plate, respectively, and co-incubated with cells for 10 days. After that, the numbers and diameter of the tumorsphere were measured in the microscopy images.

Transwell Invasion Assays. Transwell chambers with 8 mm pores were employed to detect the invasion ability of cells. In the assay, 1×10^5 HCT-116 cells in 200 μL of serum-free medium were introduced into the upper compartment, and 500 μL of DMEM enriched with 10% FBS as a chemoattractant was introduced into the lower compartment. After inoculation with vehicle (DMSO), **CX-4945** (5 μM), and **1c** (5 μM) for 24 h, a cotton swab was employed to remove the HCT-116 cells on the upper surface of the inserted membrane. Crystal violet staining was performed on the HCT-116 cells on the lower surface of the inserted membrane for 30 min. Lastly, an inverted microscope was employed to image the number of cells on the lower surface of the membrane.

Cell Apoptotic Assay. An Annexin V-FITC apoptotic detection kit was employed to explore the apoptosis of HCT-116 cells induced by vehicle (DMSO), **CX-4945** (5 μM), and **1c** (5, 10 and 20 μM). We collected the HCT-116 cells in the log growth phase and suspended them in DMEM enriched with 10% FBS. A total of 2×10^5 cells/well were inoculated in a six-well plate and left to adhere overnight. Then, the original growth medium was discarded, and fresh medium was added and treated with the compounds under study, respectively, for 24 h at 37 °C. The cells were inoculated with Annexin V-FITC followed by PI in the dark for 10 min at room temperature. Afterward, the cells were assessed by flow cytometry, and the apoptotic value was obtained by the Cell-Quest software (BD Biosciences).

Cell Cycle Arrest Assay. The HCT-116 cells were diluted into 2×10^5 cells/mL mixed liquid with DMEM with 10% FBS, inoculated in a six-well plate, and grown at 37 °C for 12 h. Then, the cancer cells were treated with vehicle (DMSO), **CX-4945** (20 μM), and **1c** (20 μM) for 24 h. The cells in each group were collected into a 5 mL centrifuge tube, about 500 μL of 70% ethanol was added, and the cells were placed in a refrigerator at −20 °C for 12 h. Subsequently, the supernatant was removed, treated with RnaseA (100 μg/mL) at 37 °C for 20 min, and stained with 1 mg/mL PI for 30 min in the dark at 4 °C. The sample was assayed by flow cytometry, and the data were analyzed with the FlowJo software (TreeStar, Inc.).

Western Blot Assay. The HCT-116 cells were diluted into 2×10^5 cells/mL mixed liquid with DMEM with 10% FBS, planted in a six-well plate, and grown at 37 °C for 12 h. The cells were treated with **CX-4945** (20 μM), **1c** (20 μM), and vehicle (DMSO) for 24 h; collected; centrifuged; and rinsed twice in PBS. Thereafter, the lysis buffer was employed to lyse the cells for 30 min on ice. The cells were then spun at 15,000 rpm for 15 min at 4 °C. The BCA protein assay reagents (Imgenex, USA) were employed to quantify the proteins as described by the manufacturer. Next, the proteins were fractionated on 10% SDS-PAGE gels and blotted onto a PVDF membrane (GE Healthcare). After that, 5% nonfat milk in the TBST buffer was employed to block the membrane, which was subsequently co-inoculated with primary antibodies (p-$Akt1^{S129}$, Akt, p-$Cdc37^{S13}$, Cdc37, p-GSK-3β(ser9), GSK-3β, DKK1, β-catenin, Cyt c, Bax, Bcl-2, pro-caspase 9, cleaved caspase 9, pro-caspase 3, cleaved caspase 3, total PARP, cleaved PARP, and β-actin) at 4 °C overnight. Thereafter, the membranes were incubated with the HRP-labeled secondary antibodies for 2 h and rinsed thrice in the TBST buffer for 15 min, and a chemiluminescence reagent (Thermo Fisher Scientifics Ltd.) was employed to visualize the protein bands.

Thermodynamic Solubility (Shake Flask Method). **1c** was added into 2 mL glass vials prior to the addition of pH 6.8 phosphate buffer to obtain a nominal concentration of 2 mg/mL. The samples were sonicated for 10 min and shaken overnight at 800 rpm (Titrimax 1000, Heidolph) at room temperature. A first phase separation of supernatant and undissolved solid was performed by centrifugation at 5000 rpm for 20 min (Eppendorf Centrifuge 5804). The supernatant was then transferred into a conical glass vial for a second centrifugation. An adequate dilution was made using the particle-free supernatant, and the concentration was quantified by LC-HRMS using a six-point calibration curve (Vanquish coupled to an Exactive-Plus, Thermo Scientific). The final determination of the solubility of **1c** in phosphate buffer solution with pH = 6.8 was 0.89 mg/mL.

Pharmacokinetic Assay. The pharmacokinetic profile of **1c** was assessed in overnight-fasted male SD rats after a single oral dose (po). **1c** was dissolved in 5% CMC-Na, and the positive control of **CX-4945·Na** was a sodium salt formulated in phosphate buffer for the rats. Six male SD rats (three for each leg) weighing about 250−270 g were clustered randomly into two groups and administered with **1c** (25 mg/kg) and **CX-4945·Na** (25 mg/kg), respectively. We collected blood samples from all the rats at 0.25, 0.50, 0.75, 1, 2, 3, 4, 6, 8, 12, 24, and 48 h post oral dosing. The blood samples were centrifuged at 4000 rpm for 10 min, and the plasma was collected and stored at −40 °C. LC−MS/MS was employed to analyze the sample. The data of blood concentration (c)−time (T) measured after oral administration were processed by the Das 2.0 software. The appropriate mathematical model was selected to fit, and the pharmacokinetic parameters were calculated.

Preparation of standard curves: 10 μL of blank plasma was added to the standard solution of **1c** or **CX-4945·Na** at different concentrations (30, 60, 150, 300, 600, 1500, 3000, 6000, 15,000, and 30,000 ng/mL), respectively, to prepare plasma samples equivalent to ropivacaine with plasma mass concentrations of 3, 6, 15, 30, 60, 150, 300, 600, 1500, and 3000 ng/mL. The LC−MS/MS technique was used to analyze the samples with different concentrations (5 μL), the ratio Y of the peak area of each component to the internal standard peak area was used to perform linear regression operation on the plasma mass concentration X, and the regression equation obtained was the standard curve. The regression equations of **1c** and **CX-4945·Na** are $Y = 0.116X - 0.00140$ ($r = 0.9986$) and $Y = 0.704X + 0.000548$ (r = 0.9968), respectively, and the minimum quantitative limit is 3 ng/mL.

Antitumor Activity Assay. Animal studies were performed as per the relevant laws and institutional guidelines set by the Jiangsu Province Committee of Use and Care of Laboratory Animals, and all protocols were approved by the Institutional Animal Care and Use Committee of Southeast University. The antitumor efficacy of **1c** was investigated in HCT-116 xenograft tumor models in nude mice. A total of 0.2 mL of 5×10^7 cell/mL cell suspension was taken and injected into the right armpit of 5-week-old male BALB/c athymic nude mice weighing about 16−18 g (purchased from Shanghai Sipo-Bikai Laboratory Animal Co. Ltd. (Shanghai, China)). When the tumors reached a volume of about 100 mm^3 in all mice, they were grouped randomly into four groups of five mice and treated *via* intragastric administration with 0.1 mL 5% glucose injection (twice a day for 4 weeks), **CX-4945·Na** (60 mg/kg, twice a day for 4 weeks), and **1c** (60 and 90 mg/kg, twice a day for 4 weeks). **CX-4945·Na** was dissolved in 25 mM NaH_2PO_4 solution, and **1c** was dissolved in 5% CMC-Na. Tumor volumes along with body weights were recorded twice a week. The calculation formula of tumor volume (TV, mm^3) is $TV = 0.5 \times \text{length} \times \text{width}^2$. The average tumor volume within each experimental group at the set time points was employed to plot growth curves *via* Origin 9.0. We sacrificed 20 mice after the last treatment, and then the tumor weight was determined as the antitumor activity of the respective groups. The heart, liver, spleen, lung, kidney, and tumor tissues were excised for HE staining. The body weight along with physical state of the mice was determined simultaneously as an indicator of systemic toxicity.

https://doi.org/10.1021/acs.jmedchem.1c00131
J. Med. Chem. 2021, 64, 5082−5098

Statistical Analysis. The data are given as means ± SD from at least three independent experiments, each in triplicate samples for individual treatment or dosage. Statistical analyses were conducted using an unpaired, two-tailed Student's *t* test. $^{*}P < 0.05$ and $^{**}P < 0.01$ signified statistical significance.

■ ASSOCIATED CONTENT

Supporting Information

The Supporting Information is available free of charge at https://pubs.acs.org/doi/10.1021/acs.jmedchem.1c00131.

Synthetic route of **BTE** and **CX-4945**, representative flow cytometry figures from the Aldefluor assays, docking of **1c** into ALDH1A1 (PDB ID: 4x4l) kinase X-ray crystal structure, Annexin CD44-FITC and CD133-PI staining results of **1c** in the HCT-116^{ALDH+} cells, HE staining internal organs and tumor tissues in the animal xenograft model of HCT-116, the inhibitory rate of the synthesized compounds on PC-3, HCT-116, MCF-7, HT-29, T24, and LO2 cells at different concentrations, the inhibitory rate of the synthesized compounds on CK2 and Clk2 at different concentrations, schematic diagram of the inhibition activity detection of compounds against CK2 and Clk2, table of the percent inhibition of compound **1c** against 208 kinases, table of the primer sequences used for qRT-PCR, table of the *in vivo* blood concentration results of **CX-4945·Na** and **1c**, table of the inhibitory effects of the measured samples on the HCT-116 cancer cell xenograft mice model, figures of ^{1}H and ^{13}C NMR, HR-MS spectra, and RP-HPLC chromatograms (PDF)

Molecular formula strings (CSV)

PDB file of **1c**-CK2α (PDB ID: 6isj) (PDB)

PDB file of **1c**-Clk2 (PDB ID: 6khe) (PDB)

PDB file of **1c**-ALDH1A1 (PDB ID: 4x4l) (PDB)

■ AUTHOR INFORMATION

Corresponding Author

Shaohua Gou − *Jiangsu Province Hi-Tech Key Laboratory for Biomedical Research and Pharmaceutical Research Center and School of Chemistry and Chemical Engineering, Southeast University, Nanjing 211189, PR China;* orcid.org/0000-0003-0284-5480; Email: 2219265800@qq.com

Authors

Yuanjiang Wang − *Jiangsu Province Hi-Tech Key Laboratory for Biomedical Research and Pharmaceutical Research Center and School of Chemistry and Chemical Engineering, Southeast University, Nanjing 211189, PR China*

Zhaodan Lv − *Pharmaceutical Research Center and School of Chemistry and Chemical Engineering, Southeast University, Nanjing 211189, PR China*

Feihong Chen − *Jiangsu Province Hi-Tech Key Laboratory for Biomedical Research and Pharmaceutical Research Center and School of Chemistry and Chemical Engineering, Southeast University, Nanjing 211189, PR China*

Xing Wang − *Pharmaceutical Research Center and School of Chemistry and Chemical Engineering, Southeast University, Nanjing 211189, PR China*

Complete contact information is available at: https://pubs.acs.org/10.1021/acs.jmedchem.1c00131

Notes

The authors declare no competing financial interest.

■ ACKNOWLEDGMENTS

We would like to thank the National Natural Science Foundation of China (Project No. 22077015); Graduate Research and Innovation Fund of Jiangsu Province, China (Project No. KYCX19_0102); and Fundamental Research Funds for the Central Universities (Project 2242020 K30059) for financial aid to this work. The authors are thankful to ICE Bioscience Inc. (Beijing) for undertaking the detection experiment of kinase spectrum. Nanjing Biorn Life Science Co. Ltd. is acknowledged for the *in vivo* tests.

■ ABBREVIATIONS

AKT, protein kinase; ALDH1A1, aldehyde dehydrogenase 1A1; Bcl-2, B-cell lymphoma-2 protein; Bax, Bcl-2 associated X protein; CSC, cancer stem cell; DIPEA, *N*,*N*-diisopropylethylamine; DMEM, Dulbecco's modified Eagle's medium; CMC-Na, sodium carboxymethyl cellulose; Cyt c, cytochrome C; EGFR, epidermal growth factor receptor; FACS, fluorescence-activated cell sorting; FBA, fetal bovine serum; FITC, fluorescein isothiocyanate isomer; GSK-3β, glycogen synthase kinase-3β; HCT-116, human colon cancer cell line; HT-29, human colon cancer cell line; HR-MS, high-resolution mass spectrometry; PC-3, human prostate cancer cell line; PI, propidium iodide; PLK1, polo-like kinase 1; LO2, human normal hepatocytes cell line; MCF-7, human breast cancer cell line; PARP, poly ADP-ribose polymerase; qRT-PCR, quantitative real-time PCR; RBITC, rhodamine B isothiocyanate; RPMI-1640, Roswell Park Memorial Institute-1640; SDSPAGE, sodium dodecyl sulfate polyacrylamide gel electrophoresis; S100A4, S100 calcium binding protein A4; TMS, tetramethylsilane; T24, human bladder cancer cell line; ZAP70, 70-kDa zeta-associated protein.

■ REFERENCES

(1) Hashimoto, A.; Gao, C.; Mastio, J.; Kossenkov, A.; Abrams, S. I.; Purandare, A. V.; Desilva, H.; Wee, S.; Hunt, J.; Jure-Kunkel, M.; Gabrilovich, D. I. Inhibition of casein kinase 2 disrupts differentiation of myeloid cells in cancer and enhances the efficacy of immunotherapy in mice. *Cancer Res.* **2018**, *78*, 5644−5655.

(2) Guerra, B.; Issinger, O.-G. Protein kinase CK2 in human diseases. *Curr. Med. Chem.* **2008**, *15*, 1870−1886.

(3) Nitta, R. T.; Gholamin, S.; Feroze, A. H.; Agarwal, M.; Cheshier, S. H.; Mitra, S. S.; Li, G. Casein kinase 2α regulates glioblastoma brain tumor-initiating cell growth through the β-catenin pathway. *Oncogene* **2015**, *34*, 3688−3699.

(4) Zanin, S.; Borgo, C.; Girardi, C.; O'Brien, S. E.; Miyata, Y.; Pinna, L. A.; Donella-Deana, A.; Ruzzene, M. Effects of the CK2 inhibitors CX-4945 and CX-5011 on drug-resistant cells. *PLoS One* **2012**, *7*, No. e49193.

(5) Duncan, J. S.; Litchfield, D. W. Too much of a good thing: the role of protein kinase CK2 in tumorigenesis and prospects for therapeutic inhibition of CK2. *Biochim. Biophys. Acta, Proteins Proteomics* **2008**, *1784*, 33−47.

(6) Qiao, Y.; Chen, T.; Yang, H.; Chen, Y.; Lin, H.; Qu, W.; Feng, F.; Liu, W.; Guo, Q.; Liu, Z.; Sun, H. Small molecule modulators targeting protein kinase CK1 and CK2. *Eur. J. Med. Chem.* **2019**, *181*, 111581.

(7) Trembley, J. H.; Wang, G.; Unger, G.; Slaton, J.; Ahmed, K. Protein kinase CK2 in health and disease: CK2: a key player in cancer biology. *Cell. Mol. Life Sci.* **2009**, *66*, 1858−1867.

(8) Ruzzene, M.; Pinna, L. A. Addiction to protein kinase CK2: a common denominator of diverse cancer cells? *Biochim. Biophys. Acta, Proteins Proteomics* **2010**, *1804*, 499−504.
(9) Perea, S. E.; Baladrón, I.; Valenzuela, C.; Perera, Y. CIGB-300: A peptide-based drug that impairs the Protein Kinase CK2-mediated phosphorylation. *Semin. Oncol.* **2018**, *45*, 58−67.
(10) de Fusco, C.; Brear, P.; Iegre, J.; Georgiou, K. H.; Sore, H. F.; Hyvönen, M.; Spring, D. R. A fragment-based approach leading to the discovery of a novel binding site and the selective CK2 inhibitor CAM4066. *Bioorg. Med. Chem.* **2017**, *25*, 3471−3482.
(11) Xing, Y.; Wang, L.; Wang, C.; Zhang, Y.; Zhang, Y.; Hu, L.; Gao, X.; Han, L.; Yang, W. Pharmacokinetic studies unveiled the drug-drug interaction between trans-2,3,5,4′-tetrahydroxystilbene-2-O-β-d-glucopyranoside and emodin that may contribute to the idiosyncratic hepatotoxicity of polygoni multiflori radix. *J. Pharm. Biomed. Anal.* **2019**, *164*, 672−680.
(12) Buontempo, F.; McCubrey, J. A.; Orsini, E.; Ruzzene, M.; Cappellini, A.; Lonetti, A.; Evangelisti, C.; Chiarini, F.; Evangelisti, C.; Barata, J. T.; Martelli, A. M. Therapeutic targeting of CK2 in acute and chronic leukemias. *Leukemia* **2018**, *32*, 1−10.
(13) Erdreich-Epstein, A.; Singh, L. R.; Joshi, S.; Vega, F. M.; Guo, P.; Xu, J.; Groshen, S.; Ye, W.; Millard, M.; Campan, M.; Morales, G.; Garlich, J. R.; Laird, P. W.; Seeger, R. C.; Shimada, H.; Durden, D. L. Association of high microvessel $\alpha v\beta 3$ and low PTEN with poor outcome in Stage 3 neuroblastoma: rationale for using first in class dual PI3K/BRD4 inhibitor, SF1126. *Oncotarget* **2017**, *8*, 52193−52210.
(14) Zakharia, K.; Miyabe, K.; Wang, Y.; Wu, D.; Moser, C. D.; Borad, M. J.; Roberts, L. R. Preclinical in vitro and in vivo evidence of an antitumor effect of CX-4945, a casein kinase II inhibitor, in cholangiocarcinoma. *Transl. Oncol.* **2019**, *12*, 143−153.
(15) Iegre, J.; Brear, P.; de Fusco, C.; Yoshida, M.; Mitchell, S. L.; Rossmann, M.; Carro, L.; Sore, H. F.; Hyvönen, M.; Spring, D. R. Second-generation CK2α inhibitors targeting the αD pocket. *Chem. Sci.* **2018**, *9*, 3041−3049.
(16) Kim, H.; Choi, K.; Kang, H.; Lee, S.-Y.; Chi, S.-W.; Lee, M.-S.; Song, J.; Im, D.; Choi, Y.; Cho, S. Identification of a novel function of CX-4945 as a splicing regulator. *PLoS One* **2014**, *9*, No. e94978.
(17) Siddiqui-Jain, A.; Drygin, D.; Streiner, N.; Chua, P.; Pierre, F.; O'Brien, S. E.; Bliesath, J.; Omori, M.; Huser, N.; Ho, C.; Proffitt, C.; Schwaebe, M. K.; Ryckman, D. M.; Rice, W. G.; Anderes, K. CX-4945, an orally bioavailable selective inhibitor of protein kinase CK2, inhibits prosurvival and angiogenic signaling and exhibits antitumor efficacy. *Cancer Res.* **2010**, *70*, 10288−10298.
(18) Cruise, E. An investigation of the CK2-dependent phosphoproteome using inhibitor refractory CK2-alpha. *Electronic Thesis and Dissertation Repository* **2017**.
(19) Karaman, M. W.; Herrgard, S.; Treiber, D. K.; Gallant, P.; Atteridge, C. E.; Campbell, B. T.; Chan, K. W.; Ciceri, P.; Davis, M. I.; Edeen, P. T.; Faraoni, R.; Floyd, M.; Hunt, J. P.; Lockhart, D. J.; Milanov, Z. V.; Morrison, M. J.; Pallares, G.; Patel, H. K.; Pritchard, S.; Wodicka, L. M.; Zarrinkar, P. P. A quantitative analysis of kinase inhibitor selectivity. *Nat. Biotechnol.* **2008**, *26*, 127−132.
(20) Cohen, P. The development and therapeutic potential of protein kinase inhibitors. *Curr. Opin. Chem. Biol.* **1999**, *3*, 459−465.
(21) Asadzadeh, Z.; Mansoori, B.; Mohammadi, A.; Aghajani, M.; Haji-Asgarzadeh, K.; Safarzadeh, E.; Mokhtarzadeh, A.; Duijf, P. H. G.; Baradaran, B. microRNAs in cancer stem cells: biology, pathways, and therapeutic opportunities. *J. Cell. Physiol.* **2019**, *234*, 10002−10017.
(22) Pattabiraman, D. R.; Weinberg, R. A. Tackling the cancer stem cells — what challenges do they pose? *Nat. Rev. Drug Discovery* **2014**, *13*, 497−512.
(23) Martins-Neves, S. R.; Cleton-Jansen, A.-M.; Gomes, C. M. F. Therapy-induced enrichment of cancer stem-like cells in solid human tumors: where do we stand? *Pharmacol. Res.* **2018**, *137*, 193−204.
(24) Tirino, V.; Desiderio, V.; Paino, F.; De Rosa, A.; Papaccio, F.; La Noce, M.; Laino, L.; De Francesco, F.; Papaccio, G. Cancer stem cells in solid tumors: an overview and new approaches for their isolation and characterization. *FASEB J.* **2013**, *27*, 13−24.
(25) Hanahan, D.; Weinberg, R. A. Hallmarks of cancer: The next generation. *Cell* **2011**, *144*, 646−674.
(26) Michael, F.; Clarke, M. D. Clinical and therapeutic implications of cancer stem cells. *N. Engl. J. Med.* **2019**, *380*, 2237−2245.
(27) Liu, J.; Tan, Y.; Zhang, H.; Zhang, Y.; Xu, P.; Chen, J.; Poh, Y.-C.; Tang, K.; Wang, N.; Huang, B. Soft fibrin gels promote selection and growth of tumorigenic cells. *Nat. Mater.* **2012**, *11*, 734−741.
(28) Kaipio, K.; Chen, P.; Roering, P.; Huhtinen, K.; Mikkonen, P.; Östling, P.; Lehtinen, L.; Mansuri, N.; Korpela, T.; Potdar, S.; Hynninen, J.; Auranen, A.; Grénman, S.; Wennerberg, K.; Hautaniemi, S.; Carpén, O. ALDH1A1-related stemness in high-grade serous ovarian cancer is a negative prognostic indicator but potentially targetable by EGFR/mTOR-PI3K/aurora kinase inhibitors. *J. Pathol.* **2020**, *250*, 159−169.
(29) Pierre, F.; Chua, P. C.; O'Brien, S. E.; Siddiqui-Jain, A.; Bourbon, P.; Haddach, M.; Michaux, J.; Nagasawa, J.; Schwaebe, M. K.; Stefan, E.; Vialettes, A.; Whitten, J. P.; Chen, T. K.; Darjania, L.; Stansfield, R.; Anderes, K.; Bliesath, J.; Drygin, D.; Ho, C.; Omori, M.; Proffitt, C.; Streiner, N.; Trent, K.; Rice, W. G.; Ryckman, D. M. Discovery and SAR of 5-(3-chlorophenylamino)benzo[c][2,6]-naphthyridine-8-carboxylic acid (CX-4945), the first clinical stage inhibitor of protein kinase CK2 for the treatment of cancer. *J. Med. Chem.* **2011**, *54*, 635−654.
(30) Hopkins, A. L.; Keserü, G. M.; Leeson, P. D.; Rees, D. C.; Reynolds, C. H. The role of ligand efficiency metrics in drug discovery. *Nat. Rev. Drug Discovery* **2014**, *13*, 105−121.
(31) Zhang, S.; Long, H.; Yang, Y.-L.; Wang, Y.; Hsieh, D.; Li, W.; Au, A.; Stoppler, H. J.; Xu, Z.; Jablons, D. M.; You, L. Inhibition of CK2α down-regulates Notch1 signalling in lung cancer cells. *J. Cell. Mol. Med.* **2013**, *17*, 854−862.
(32) Kozovska, Z.; Patsalias, A.; Bajzik, V.; Durinikova, E.; Demkova, L.; Jargasova, S.; Smolkova, B.; Plava, J.; Kucerova, L.; Matuskova, M. ALDH1A inhibition sensitizes colon cancer cells to chemotherapy. *BMC Cancer* **2018**, *18*, 656.
(33) Chen, J.-J.; Cai, N.; Chen, G.-Z.; Jia, C.-C.; Qiu, D.-B.; Du, C.; Liu, W.; Yang, Y.; Long, Z.-J.; Zhang, Q. The neuroleptic drug pimozide inhibits stem-like cell maintenance and tumorigenicity in hepatocellular carcinoma. *Oncotarget* **2017**, *8*, 17593−17609.
(34) Lu, Y.; Zhu, H.; Shan, H.; Lu, J.; Chang, X.; Li, X.; Lu, J.; Fan, X.; Zhu, S.; Wang, Y.; Guo, Q.; Wang, L.; Huang, Y.; Zhu, M.; Wang, Z. Knockdown of Oct4 and Nanog expression inhibits the stemness of pancreatic cancer cells. *Cancer Lett.* **2013**, *340*, 113−123.
(35) Basati, G.; Mohammadpour, H.; Emami Razavi, A. Association of high expression levels of Sox_2, Nanog, and Oct4 in gastric cancer tumor tissues with progression and poor prognosis. *J. Gastrointest. Surg.* **2020**, *51*, 41−47.
(36) Perugorria, M. J.; Olaizola, P.; Labiano, I.; Esparza-Baquer, A.; Marzioni, M.; Marin, J. J. G.; Bujanda, L.; Banales, J. M. Wnt−β-catenin signalling in liver development, health and disease. *Nat. Rev. Gastroenterol. Hepatol.* **2019**, *16*, 121−136.
(37) Hanahan, D.; Weinberg, R. A. The hallmarks of cancer. *Cell* **2000**, *100*, 57−70.
(38) Wang, W.; Yi, M.; Chen, S.; Li, J.; Zhang, H.; Xiong, W.; Li, G.; Li, X.; Xiang, B. NOR1 suppresses cancer stem-like cells properties of tumor cells *via* the inhibition of the AKT-GSK-3β-Wnt/β-catenin-ALDH1A1 signal circuit. *J. Cell. Physiol.* **2017**, *232*, 2829−2840.
(39) Cohen, P.; Goedert, M. GSK3 inhibitors: development and therapeutic potential. *Nat. Rev. Drug Discovery* **2004**, *3*, 479−487.
(40) Mills, C. N.; Nowsheen, S.; Bonner, J. A.; Yang, E. S. Emerging roles of glycogen synthase kinase 3 in the treatment of brain tumors. *Front. Mol. Neurosci.* **2011**, *4*, 47.
(41) Chua, P. C.; Haddach, M.; Nagasawa, J. Y.; Pierre, F. Preparation of substituted pyrimidoquinolines and thienoquinolines as serine-threonine protein kinase and PARP modulators. Sep 3, 2009, WO 2009108912 A1.

https://doi.org/10.1021/acs.jmedchem.1c00131
J. Med. Chem. 2021, 64, 5082−5098

(42) Livak, K. J.; Schmittgen, T. D. Analysis of relative gene expression data using Real-time quantitative PCR and the $2^{-\Delta\Delta CT}$ method. *Methods* **2001**, *25*, 402−408.

https://doi.org/10.1021/acs.jmedchem.1c00131
J. Med. Chem. 2021, 64, 5082−5098